Report No. FHWA-KS-14-03 ▪ FINAL REPORT▪ October 2014

Enhancement of Welded Steel Bridge Girders Susceptible to Distortion-Induced Fatigue

Caroline Bennett, Ph.D., P.E.
Adolfo Matamoros, Ph.D.
Ron Barrett-Gonzalez, Ph.D.
Stan Rolfe, Ph.D., P.E.

The University of Kansas Center for Research, Inc.

A Transportation Pooled Fund Study - TPF-5(189)

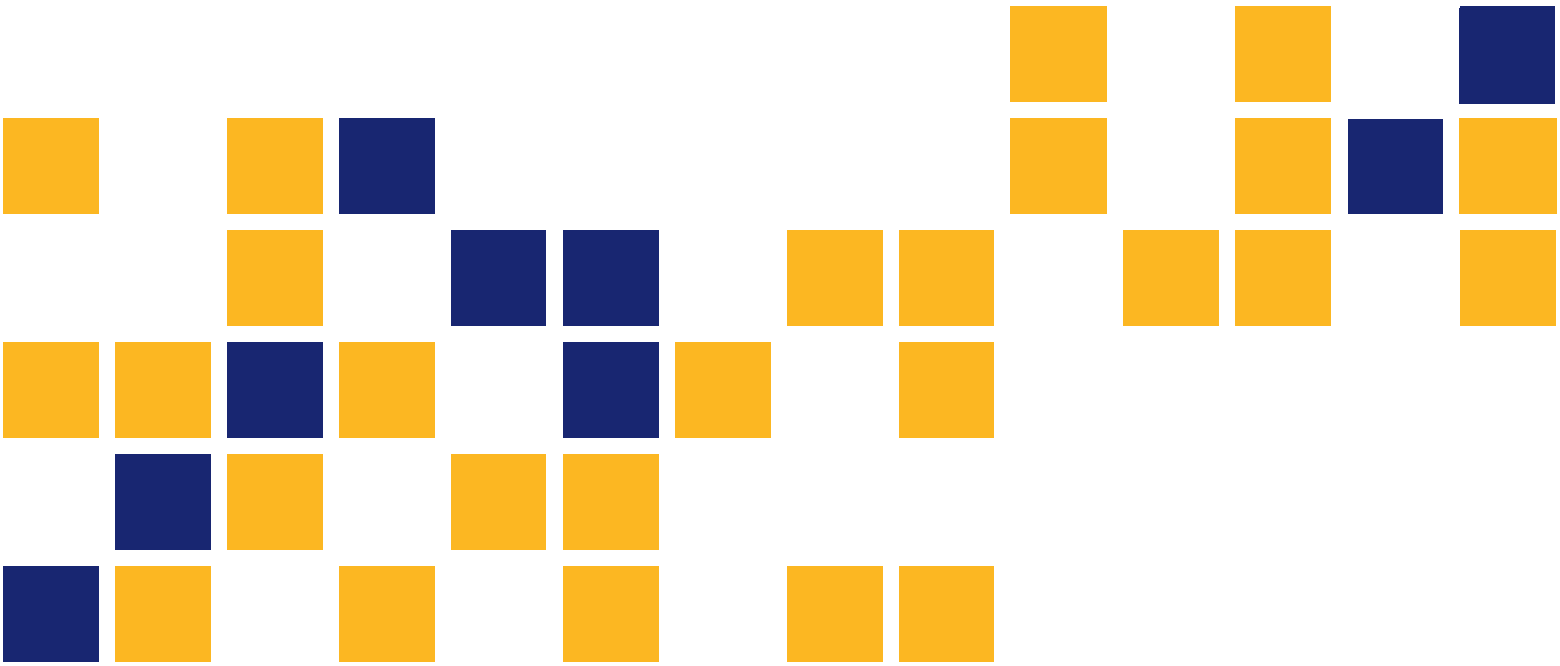

Kansas Department of Transportation

This page intentionally left blank.

1 Report No. FHWA-KS-14-03	**2 Government Accession No.**	**3 Recipient Catalog No.**
4 Title and Subtitle Enhancement of Welded Steel Bridge Girders Susceptible to Distortion-Induced Fatigue		**5 Report Date** October 2014 **6 Performing Organization Code** TPF-5(189)
7 Author(s) Caroline Bennett, Ph.D., P.E., Adolfo Matamoros, Ph.D., Ron Barrett-Gonzalez, Ph.D., and Stan Rolfe, Ph.D., P.E.		**7 Performing Organization Report No.** SM Report No. 106
9 Performing Organization Name and Address The University of Kansas Center for Research, Inc. 2385 Irving Hill Road – Campus West Lawrence, Kansas 66045		**10 Work Unit No. (TRAIS)** **11 Contract or Grant No.** C1795
12 Sponsoring Agency Name and Address Kansas Department of Transportation Bureau of Research 2300 SW Van Buren Topeka, Kansas 66611-1195		**13 Type of Report and Period Covered** Final Report September 2008 – June 2014 **14 Sponsoring Agency Code** RE-0510-01 & TPF-5(189)

15 Supplementary Notes
For more information write to address in block 9. Pooled Fund Study TPF-5(189) sponsored by the following DOTs: Kansas, California, Iowa, Illinois, Louisiana DOTD, New Jersey, New York State, Oregon, Pennsylvania, Tennessee, Washington State, Wisconsin and Wyoming.
Appendices are available in a separate PDF. http://ksdot1.ksdot.org/burmatrres/kdotlib2.asp or library@ksdot.org

The goal of this study was to develop and evaluate the performance of retrofit techniques for existing steel bridges that have already sustained damage due to distortion-induced fatigue, or are anticipated to experience distortion-induced fatigue cracking within their design life. A second goal was to evaluate the use of new technologies and materials for repairing distortion-induced fatigue damage in steel bridges.

While a number of retrofit techniques exist for repairing distortion-induced fatigue cracking, many of them require partial or full bridge closure to perform the repair. The retrofits developed under this project are intended to be able to be installed with minimal disturbance to traffic. Four primary subject matters are reported on within this document: (1) the development of the "angles-with-plate" distortion-induced fatigue repair; (2) development of fiber reinforced polymer (FRP) repairs for distortion-induced fatigue and in-plane fatigue; (3) development of Piezoelectric Induced Compressive Kinetics (PICK) technology for treatment of crack-arrest holes; and (4) a series of analytical investigations aimed at better understanding distortion-induced fatigue susceptibility of skewed bridge systems.

17 Key Words Bridge Girders, Fatigue, Structures, and Welded Steel		**18 Distribution Statement** No restrictions. This document is available to the public through the National Technical Information Service www.ntis.gov.	
19 Security Classification (of this report) Unclassified	**20 Security Classification (of this page)** Unclassified	**21 No. of pages** 96	**22 Price**

Form DOT F 1700.7 (8-72)

This page intentionally left blank.

Enhancement of Welded Steel Bridge Girders Susceptible to Distortion-Induced Fatigue

Final Report

Prepared by

Caroline Bennett, Ph.D., P.E.
Adolfo Matamoros, Ph.D.
Ron Barrett-Gonzalez, Ph.D.
Stan Rolfe, Ph.D., P.E.
The University of Kansas Center for Research, Inc.

A Report on Research Sponsored by

THE KANSAS DEPARTMENT OF TRANSPORTATION
TOPEKA, KANSAS

and

THE UNIVERSITY OF KANSAS CENTER FOR RESEARCH, INC.
LAWRENCE, KANSAS

October 2014

NOTICE

The authors and the state of Kansas do not endorse products or manufacturers. Trade and manufacturers names appear herein solely because they are considered essential to the object of this report.

This information is available in alternative accessible formats. To obtain an alternative format, contact the Office of Public Affairs, Kansas Department of Transportation, 700 SW Harrison, 2nd Floor – West Wing, Topeka, Kansas 66603-3745 or phone (785) 296-3585 (Voice) (TDD).

DISCLAIMER

The contents of this report reflect the views of the authors who are responsible for the facts and accuracy of the data presented herein. The contents do not necessarily reflect the views or the policies of the state of Kansas. This report does not constitute a standard, specification or regulation.

Abstract

This report presents the findings of Transportation Pooled Fund Study TPF-5(189), "Enhancement of Welded Steel Bridge Girders Susceptible to Distortion-Induced Fatigue." The goal of TPF-5(189) was to develop and evaluate the performance of retrofit techniques for existing steel bridges that have already sustained damage due to distortion-induced fatigue, or are anticipated to experience distortion-induced fatigue cracking within their design life. A second goal of the study was to evaluate the use of new technologies and materials for repairing distortion-induced fatigue damage in steel bridges.

While a number of retrofit techniques exist for repairing distortion-induced fatigue cracking, many of them require partial or full bridge closure to perform the repair. The retrofits developed under TPF-5(189) are intended to be able to be installed with minimal disturbance to traffic. Four primary subject matters are reported on within this document: (1) the development of the "angles-with-plate" distortion-induced fatigue repair; (2) development of fiber reinforced polymer (FRP) repairs for distortion-induced fatigue and in-plane fatigue; (3) development of Piezoelectric Induced Compressive Kinetics (PICK) technology for treatment of crack-arrest holes; and (4) a series of analytical investigations aimed at better understanding distortion-induced fatigue susceptibility of skewed bridge systems.

This report is intended to provide a comprehensive overview of the work performed under TPF-5(189). The remainder of the report is structured into four Appendices (A, B, C, and D). The summary provided in the report refers the reader to appropriate parts within the Appendices for detailed explanations and analysis. Appendix A covers development of the angles-with-plate repair, Appendix B covers the multiple FRP repairs developed, Appendix C covers the PICK technology developed and Appendix D covers the analytical investigations regarding skewed steel bridge systems. The four appendices represent an edited and abridged collection of work originating from student theses and paper manuscripts created under TPF-5(189), and are intended as stand-alone documents, but are richer in the context of the other sections within that particular appendix.

Acknowledgements

The authors of this report would like to gratefully acknowledge the agencies that supported the work done under Transportation Pooled Fund Study TPF-5(189): the Kansas DOT (KDOT), Caltrans, the FHWA, the Iowa DOT, the Illinois DOT, the Louisiana DOTD, the New Jersey DOT, the New York State DOT, the Oregon DOT, the Pennsylvania DOT, the Tennessee DOT, the Washington State DOT, the Wisconsin DOT, and the Wyoming DOT.

The authors are especially grateful to the lead agency, KDOT, for their support of the work performed under this project, and for knowledgeable guidance and input provided by Mr. Loren Risch, Mr. John Jones, Mr. Calvin Reed, and Mr. Paul Kulseth throughout the project activities.

The authors would also like to thank the University of Kansas Transportation Research Institute (KU TRI) and the KU School of Engineering for their support of this project.

Finally, the authors are grateful to the many graduate and undergraduate students who have contributed their talents to this project, especially: Ms. Amanda Hartman, Mr. Fatih Alemdar, Mr. Gary Simmons, Ms. Katie McElrath, Ms. Temple Richardson, Ms. Regan Gangel, Mr. Daniel Nagati, Mr. Joshua Crain, Mr. Chris Adams, and Mr. Jack Przywara.

Table of Contents

Due to file size, Appendices A to D are available in a separate file located at:

http://ksdot1.ksdot.org/burmatrres/kdotlib2.asp

or by contacting the KDOT Library at library@ksdot.org or 785-291-3463.

List of Tables

List of Figures

Chapter 1: Introduction

Distortion-induced fatigue is a serious problem across the national bridge inventory, affecting many steel bridges designed before the mid-1980s. Connor and Fisher (2006) have estimated that as many as 90% of fatigue-related cracks in steel bridges are due to distortion-induced fatigue. Because distortion-induced fatigue tends to develop in bridge connection details, near transverse elements such as cross-frames and diaphragms, repairing distortion-induced fatigue damage can be a difficult task, especially when the affected detail is near the intersection of the top flange, connection plate, and web.

The region of a girder defined by the truncation of a connection plate and the web is often referred to as a "web gap," a detail that has been found to be highly susceptible to distortion-induced fatigue. Web gaps are formed when a connection plate is framed in the web, but not connected to the adjacent flanges(s). Before the mid-1980s this was common practice; neglecting to weld the connection plate to the adjacent tension flange was believed to be good fatigue detailing practice, avoiding the introduction of a detail susceptible to fatigue damage in the tension flange. Unfortunately, this practice resulted in the unintended consequence of introducing a detail highly susceptible to fatigue damage in the web region, between the termination of the connection plate and the flange, as depicted in Figure 1.1. As forces are transferred through the transverse elements (cross-frame or diaphragm), the load path results in large stresses being induced in the highly-flexible web gap area. Cracks tend to form around the connection plate-to-web weld and the web-to-flange weld. Cracking in web gaps that exist near the top flange of a girder are especially difficult to repair given that the top surface of the flange is inaccessible due to the presence of a concrete deck.

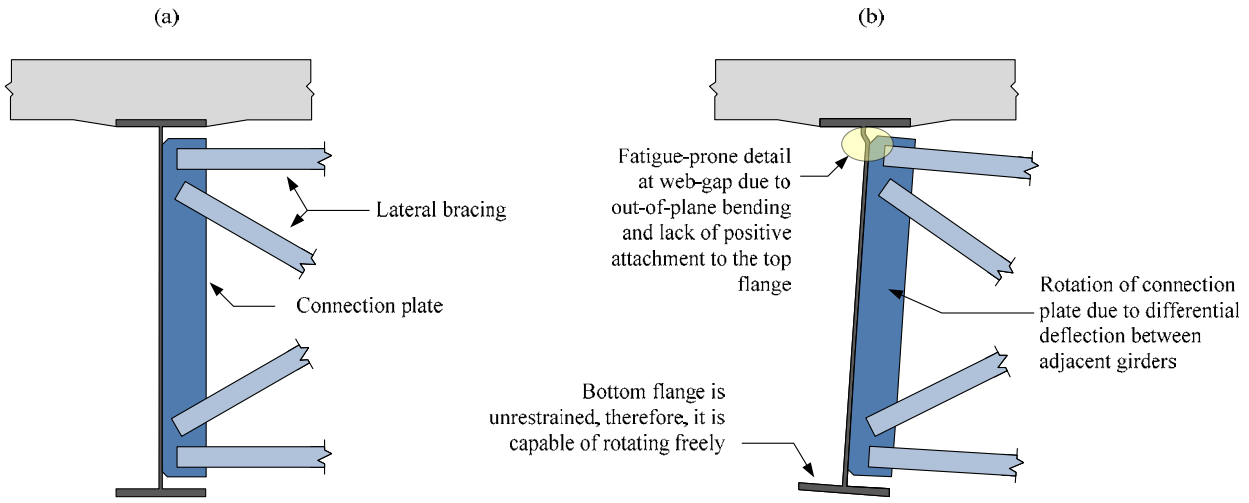

Figure 1.1: Depiction of distortion-induced fatigue mechanism in a steel bridge girder

Departments of Transportation (DOTs) have taken numerous approaches to repairing cracked web gap regions in the past, with varied degrees of success and cost – both in terms of dollars and inconvenience to the traveling public. One retrofit technique that has been commonly used is a pair of angles welded to the connection plate by one leg and bolted to the adjacent flange through the other leg, providing a positive connection between the connection plate and the flange (Figure 1.2). To-date, this technique has arguably shown the best results improving the fatigue performance of susceptible bridges. The main drawback of this repair is that it is expensive and difficult to implement when it is applied in a top web gap in the manner described. To complete the bolted connection between the angle and the flange, the top surface of the flange must be accessed. In most cases, a concrete deck will interfere with access – necessitating partial removal of the deck, resulting in partial or full closure of the bridge. In some cases, this approach may be convenient (e.g., if the bridge is scheduled for re-decking with cast-in-place reinforced concrete), and in these cases, there is little need for alternative repair options. In cases when the retrofit timing does not coincide with re-decking needs, there is a clear need for alternative repairs. Variations of this technique have been implemented by DOTs in which the connection to the top flange is made either by welding threaded studs (Jones et al. 2008) or by tapping into the inside face of the flange; however, these variations have not been rigorously researched and there is a lack of data on their effectiveness and potential fatigue ‘side effects’.

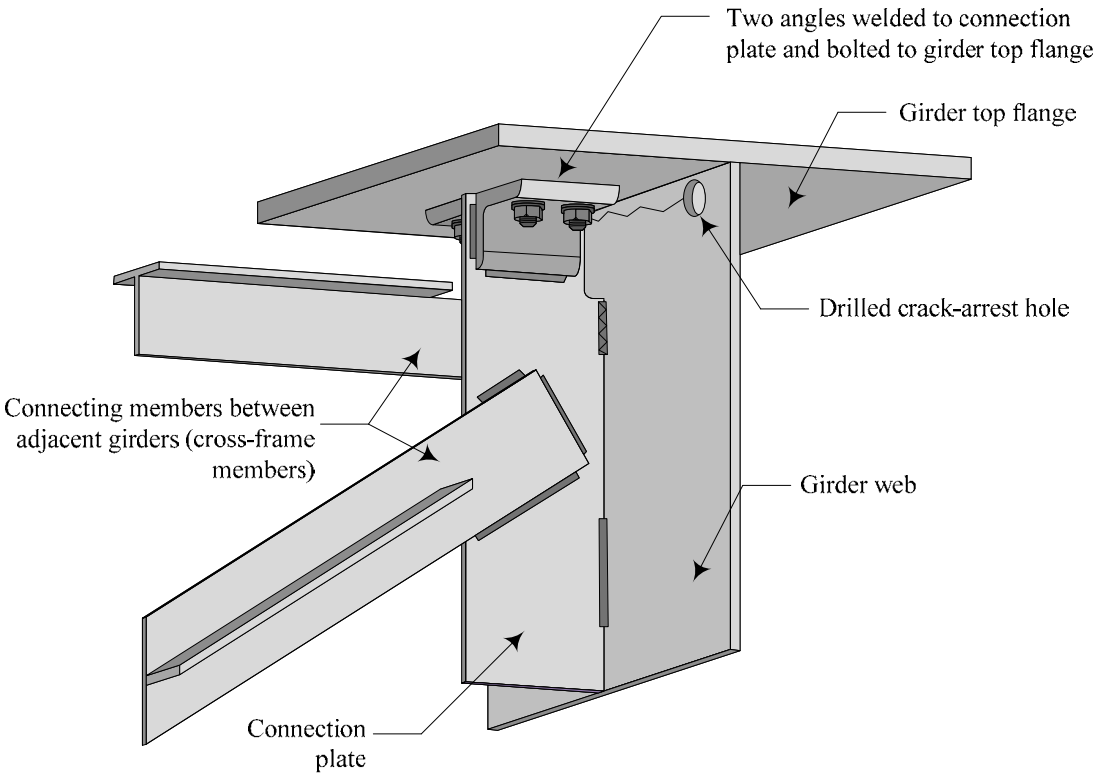

Figure 1.2: Retrofit utilizing a pair of angles connecting the connection plate to the adjacent flange

The objective of Pooled Fund Study TPF-5(189), "Enhancement of Welded Steel Bridge Girders Susceptible to Distortion-Induced Fatigue," was to improve the performance of existing steel bridge girders through application of retrofits that may be implemented with minimal disruption to traffic. A second objective was to evaluate the use of new technologies and materials to repair fatigue damage in steel bridges. This report describes a comprehensive investigation in which three primary techniques were developed with those two goals in mind: (1) a steel retrofit termed "angles-with-plate"; (2) retrofit measures relying on use of fiber reinforced polymer (FRP) materials; and (3) PICK technology. The three methods listed here are presented in order of readiness for field application, with the angles-with-plate technique the most field-ready retrofit developed under TPF-5(189). Additionally, this report describes an investigation into the effects of cross-frame placement and bridge skew angle, to aid bridge owners in repairing bridges with various geometric layouts. This investigation was undertaken

because it was recognized that it plays a significant role on the susceptibility to fatigue damage of steel bridges.

This report is intended to provide a concise summary of the methods and important findings of TPF-5(189), while the Appendices are intended to provide detailed information regarding the various efforts undertaken in TPF-5(189).

Chapter 2: Background

During the 1930s, several failures occurred in steel bridges originating from welds between connection plates and girder tension flanges (Fisher and Keating 1989). In an effort to prevent this type of fatigue damage from re-occurring, it became common practice to provide no positive attachment between connection plates and girder flanges. An unintended consequence of the lack of connection between the connection plate and adjacent flange was that a weak web gap region susceptible to out-of-plane distortions and fatigue was created.

Uneven loading of girders at equal stations along a bridge induces differential deflections between adjacent girders, causing rotation of lateral bracing members. Because the girder top flange is laterally restrained by the deck, out-of-plane displacement is concentrated in the flexible web gap region. The resulting secondary stresses in the web gap can lead to distortion-induced fatigue cracking. Although current American Association of State and Highway Transportation Officials' (AASHTO) Load and Resistance Factor Design (LRFD) Bridge Design Specifications (2013) require positive attachment between transverse stiffeners and girder flanges, many steel bridges constructed prior to the mid-1980s are at risk of experiencing damage due to distortion-induced fatigue. The following discussion is intended to provide background on the factors that influence susceptibility to distortion-induced fatigue and on the types of measures that have been used in past applications to retrofit bridges susceptible to distortion-induced fatigue.

2.1 Factors Influencing Distortion-Induced Fatigue Susceptibility in Steel Bridges

Susceptibility to distortion-induced fatigue damage is a complicated problem that is largely influenced by bridge geometry. Skew angle, span length, girder spacing, and deck thickness influence differential deflections between adjacent girders and therefore affect the potential for distortion-induced fatigue damage. Decreased span length and increased girder spacing both amplify differential deflection, except when the bridge span approaches truck length. As girder length increases and the bridge becomes increasingly flexible, lateral bracing

more effectively distributes load between girders, and the bridge displaces vertically with less differential deflection (Berglund and Schultz 2006).

Another factor that affects this problem is that bridge supports are often skewed to accommodate highway alignments. At equal stations along skewed bridges, each girder is subjected to varied bending moment and deflection under uniform loading. Differential deflections and susceptibility to distortion-induced fatigue damage tend to increase with increasing skew angle (Berglund and Schultz 2006). Skew angle also influences lateral bracing configuration.

Lateral bracing helps to distribute live loads between girders and therefore impacts the resulting differential deflections and web gap stresses in multi-girder steel bridges. There are numerous lateral bracing configurations because brace type and placement can both be varied widely. Use of cross braces instead of bent-plate diaphragms have been shown to significantly reduce maximum differential deflection (Li and Schultz 2005). Furthermore, K-type truss diaphragms have shown to create smaller secondary stresses in web gaps than X-type cross frames (Fisher et al. 1990).

Multiple brace layouts may be used in skewed bridges, including braces placed parallel to the skew angle, perpendicular to the girder web, and staggered. Placing cross frames or diaphragms parallel to skew angle and directly across from each other is often the optimal solution, but not always practical. Back-to-back bracing members have a balancing effect on out-of plane bending stresses (Barth and Bowman 2001). Placing cross frames parallel to skew angle allows lateral bracing members to be attached to adjacent girders at equal points along the member where girders are subjected to equal bending moments and deflection under uniform loading. At high skew angles, braces placed parallel to the skew angle tend to become excessively long and flexible and therefore less effective at distributing load. Current AASHTO-LRFD Bridge Design Specifications (2013) require that lateral bracing members in bridges with skew angles greater than 20 degrees be placed perpendicular to girder webs. In such bridges, lateral bracing can be either non-staggered or staggered. Non-staggered, back-to-back brace placement allows brace forces to utilize the balancing effect. The main drawback of this configuration is that braces are attached to different points along each girder, which increases the

amount of differential deflection between both ends of the brace. To avoid this limitation, braces are often placed in a staggered configuration.

Studies about the effect of cross frame configuration on the susceptibility to fatigue damage have yielded mix results. Fraser et al. (2000) reported that fatigue cracks were more pronounced in bridges with staggered diaphragms than in bridges with non-staggered diaphragms, but Barth and Bowman (2001) concluded the opposite.

Ongoing research at the University of Texas-Austin involves the use of half-pipe shapes instead of bent-plate transverse connection stiffeners in skewed bridges with cross frames oriented parallel to skew angle. Initial results have indicated that the proposed connection detail is much stiffer than the bent-plate connection, allowing cross frame spacing to be increased due to higher efficiency of fewer cross frames. A stiffer connection combined with a reduced number of cross frames may dramatically decrease bridge susceptibility to distortion-induced fatigue (Quadrato et al. ND).

Web gap geometry is thought to influence the amount of secondary stresses induced in the web gap region. According to a survey conducted by Fisher et al. (1990), the web gap length (the vertical dimension along the web between the inside of the flange and the weld attaching the connection stiffener to the girder web) typically ranges from 6 to 102 mm (0.25 to 4.0 in). Because web gaps must absorb the out-of-plane displacement in a relatively short, flexible region, smaller web gaps have less space and material to absorb this displacement, and the risk of distortion-induced fatigue cracking is increased with decreased web gap length (Fisher et al. 1990).

2.2 Existing Retrofit Techniques for Distortion-Induced Fatigue

An extensive ‘toolkit’ of distortion-induced fatigue repair and retrofit techniques that have been developed to enhance fatigue life of steel bridges is already in existence, including: stiffening the fatigue-susceptible region, softening the fatigue-susceptible region, or removal of connection elements. A broad overview of techniques is included here, but the reader interested in a greater level of detail is referred to Federal Highway Administration’s (FHWA) *Manual for Repair and Retrofit of Fatigue Cracks in Steel Bridges* (Dexter and Ocel 2013), which provides a cumulative listing of commonly-used retrofit techniques for distortion-induced fatigue.

Numerous studies have concluded that fatigue performance can be enhanced by either stiffening the web gap or softening the restraint on the connection, although it should be noted that little guidance is provided in the literature about which solution is more appropriate for a given bridge configuration. Fisher et al. (1990) showed that positive attachment between the connection plate and adjacent flange reduced secondary stresses in the web gap region by reducing the magnitude of out-of-plane displacement in the girders web. Positive connection can be accomplished using methods such as welds, bolts, epoxy, and/or angles. Field weld quality can be a concern if overhead welding is required. Angles or WT shapes can be attached to the connection plate and flange to reduce stress demands. Stiffness of the connection elements must also be considered because it has been shown to influence effectiveness (Connor and Fisher 2006).

Softening the level of restraint provided by the connection has also been shown to reduce stresses in the web gap region in various case studies. Loosening the bolts between a connection plate and girder web in a bolted connection may reduce both stresses and out-of-plane distortion (Khalil et al. 1998). Another softening technique involves removal of a portion of the transverse connection plate, lengthening the web gap. To accomplish this, a hole may be drilled in the connection plate and a slot flame-cut between the girder web and connection plate.

An additional method of eliminating secondary stresses in web gap regions is to remove lateral brace elements altogether. In composite bridges, lateral braces may not be required in positive bending moment regions after construction due to stability provided by the concrete deck. However, lateral bracing may still be needed at supports to transfer lateral loads. Although removal of bracing has been shown to eliminate secondary stresses in web gaps, this technique has been shown to increase differential deflections between adjacent girders by as much as 25% (Tedesco et al. 1995) and bending moments by as much as 15% (Stallings et al. 1999). Therefore, removal may not be advisable unless the bridge under consideration was designed with a high reserve capacity. Another disadvantage of lateral brace removal is that temporary bracing would be required during deck replacement.

Several methods have been shown to improve fatigue life of welds including shot peening, hammer peening, laser peening, and ultrasonic impact treatment (UIT). These weld

treatment methods aim to induce residual compressive stresses at the weld toe resulting in reduced tensile stress ranges experienced at critical details. It should be noted that these techniques are only considered to be effective when applied before cracking has initiated.

After a fatigue crack has initiated, growth can be retarded by drilling a hole at the tip of the crack, reducing the stress demand at the tip of the crack which increases fatigue life. Crack-arrest holes can be used in combination with other methods such as cold-expansion of the hole or introduction of fully-tightened bolts, which introduce compressive stresses at the edges of the hole.

Despite the fact that a significant number of retrofit methods for distortion-induced fatigue are already in existence, there is a need for the development of retrofit measures that are effective, cost-effective, and can be applied with minimal disruption to the traveling public. As new materials and technologies are developed, questions arise about the feasibility of implementing those new technologies. While some of those technologies may not be mature enough for immediate implementation, this study was intended to provide a first step to their future use by exploring the most efficient manner to use them, and to identify the major technical barriers for their implementation. Chapter 3 describes the methodology used within TPF-5(189) to develop such retrofit techniques.

Chapter 3: Methodology

Chapter 3 of this report provides an overview of the methodology used in the research conducted under TPF-5(189).

3.1 Development of Angles-with-Plate Retrofit

The angles-with-plate retrofit was developed and tested using three different techniques:

- A series of physical tests performed on 2.8 m (9.3 ft) long girder segments (Section 3.1.1);
- A series of physical tests performed on a three-girder, 9.1 m (30 ft) long steel bridge system (Section 3.1.2), and
- A series of computational simulations (Sections 3.1.3 and 3.1.4).

This approach allowed the researchers to explore the viability of a novel retrofit technique using computational simulations and a 2.8 m (9.3 ft) girder model that allowed for greater levels of test repetition and economy than the three-girder test bridge. Of all the retrofit measures developed under TPF-5(189) and discussed in this report, the angles-with-plate repair technique was perceived to be the most readily adoptable by state agencies. After refinement in computational simulations and girder model testing, the angles-with-plate retrofit technique was further tested in the three-girder 9.1 m (30 ft) long test bridge model, in which a series of 14 test trials was performed.

For brevity and clarity, a brief summary of the test methodologies for each of these three techniques are presented in the following discussion, with detailed descriptions provided in referenced parts of Appendix A.

3.1.1 Physical Testing Performed on Girder Models

The following discussion is a brief summary of the physical testing performed on the girder models. Detailed explanations of this testing sequence have been provided in Appendix A.1 and A.2.

The angles-with-plate retrofit measure was initially developed and tested on a 2.8 m (9.3 ft) long girder model loaded to cause distortion-induced fatigue damage after computational simulations demonstrated the potential for a significant improvement in performance (see Sections 3.1.3 to 3.1.4). The test configuration and girder dimensions used in this portion of the

study are presented in Figure 3.1. The girder models were tested upside-down with respect to the orientation of a bridge girder, meaning that the unrestrained flange was at the top of the subassembly, while the restrained flange was attached to the reaction floor.

The girder subassembly was cyclically loaded under a constant force range while the initiation and propagation of fatigue cracks was carefully monitored. The maximum load applied was 20 kN (4.6 kip) and the minimum was 3.6 kN (0.8 kip). These load values induced a stress range of 197 MPa (29 ksi) at the top of the web gap region. Fourteen test trials were performed using this test configuration to evaluate the performance of the angles-with-plate retrofit when applied over different crack lengths and geometries.

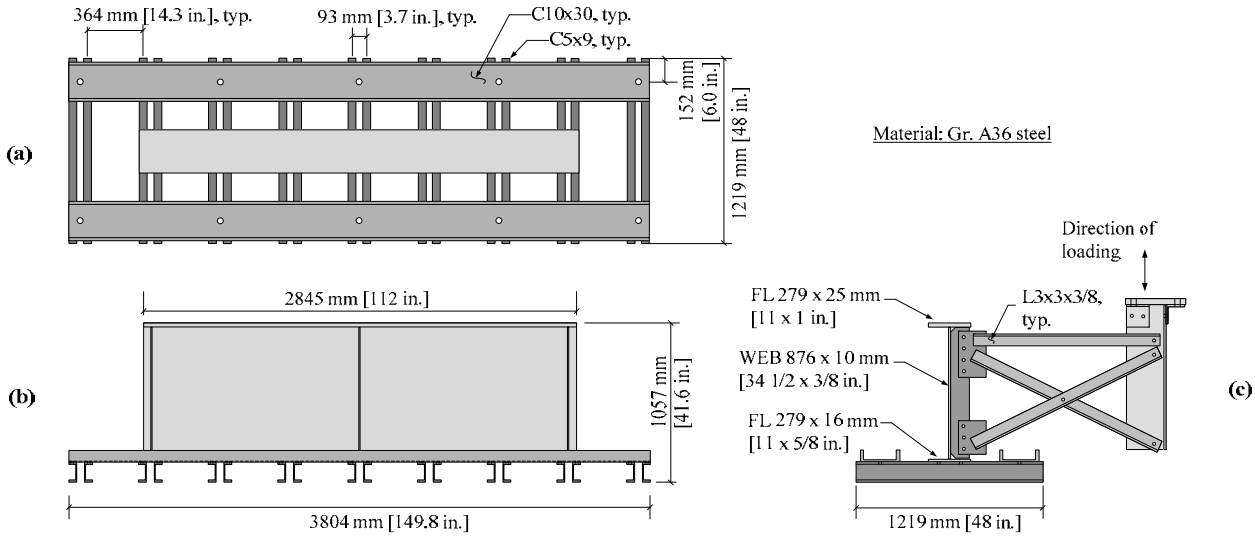

Figure 3.1: Test configuration for 2.8 m (9.3 ft) girder models loaded to cause distortion-induced fatigue damage

In the bottom web gap, the connection plate had a clipped end of 32 mm ($1^1/_4$ inch) and a 3.2 mm ($^1/_8$ inch) gap between the connection plate and bottom flange. At the top of the girder, the connection plate was fabricated as milled-to-bear against the inside face of the top flange, without any welded connection.

The girder subassembly was attached to the laboratory floor with channels connected to the girder. An X-type cross-frame connected the specimen to the actuator. The cross-frame was connected to a WT section used to stabilize the free end of the cross frame and to prevent

warping and bending of the frame while loading the specimen. All of the plates used to fabricate the built-up section were Gr. A36 steel; material properties were measured through tensile tests after the fatigue testing sequence was completed.

Specimens were instrumented with linear variable differential transformers (LVDTs) and strain gages, as shown in more detail in Appendix A.1 and A.2. Inspections for crack initiation and propagation were performed periodically during the test trials, using dye penetrant and ultraviolet (UV) light. Test trials were stopped when crack length exceeded a predefined threshold or when the number of cycles exceeded run-out, taken in these tests equal to 1.2 million cycles. Because the measured stress range was 200 MPa (29 ksi) in the web gap region before cracking initiated, run-out was defined in this study as the number of cycles in the S-N curve of the AASHTO LRFD Bridge Design Specification (AASHTO 2013) corresponding to a Category A detail (approximately 1.2 million cycles at a stress range of 200 MPa (29 ksi).

The experimental program is summarized in Table 3.1. Three specimens were evaluated with a total of 14 different test trials. Specimen 1 was fabricated to have a pre-existing horizontal crack with a length of 38 mm ($1^1/_2$ inch), positioned 17 mm (0.65 inch) from the top of the bottom flange, and was used primarily to calibrate the results of the finite element model. Specimen 2 was used to evaluate the performance of two mitigation measures, angles-with-plate and crack-arrest holes, for a given crack configuration in the web gap (a discussion of the crack-arrest holes component of this test sequence is provided in Appendix A.1 and A.2). During testing of Specimen 2, a crack was also observed in the top web gap, so tests were performed with the angles-and-plate retrofit measure in both the top and bottom web gaps. Specimen 3 was used to evaluate the effectiveness of the angles-and-plate retrofit measure for various fatigue crack lengths. During all trials, specimens were inspected periodically to measure crack growth.

Table 3.1: Experimental Program for Physical Testing Performed on Girder Segments

Specimen	Test Trial	Configuration
1	1	Pre-Cracked, Unretrofitted
2	1	Uncracked, Unretrofitted
2	2	203 mm (8 in.) Horizontal Crack Bottom Web Gap, Angles with Plate Retrofit Bottom Web Gap
2	3	203 mm (8 in.) Horizontal Crack Bottom Web Gap, 84 mm (3.3 in.) Horizontal Crack Top Web Gap, Angles with Plate Retrofit Bottom and Top Web Gap
2	4	216 mm (8.5 in.) Horizontal Crack Bottom Web Gap, 84 mm (3.3 in.) Horizontal Crack Top Web Gap, Crack-Stop Hole Retrofit
2	5	216 mm (8.5 in.) Horizontal Crack Bottom Web Gap, 84 mm (3.3 in.) Horizontal Crack Top Web Gap, Angles with Plate Retrofit Bottom and Top Web Gap
3	1	Uncracked, Unretrofitted
3	2	51 mm (2 in.) Horizontal Crack, Angles with Plate Retrofit Bottom Web Gap
3	3	51 mm (2 in.) Horizontal Crack, Unretrofitted
3	4	102 mm (4 in.) Horizontal Crack, Angles with Plate Retrofit Bottom Web Gap
3	5	102 mm (4 in.) Horizontal Crack, Unretrofitted
3	6	152 mm (6 in.) Horizontal Crack, Angles with Plate Retrofit Bottom Web Gap
3	7	152 mm (6 in.) Horizontal Crack, Unretrofitted
3	8	203 mm (8 in.) Horizontal Crack, Angles with Plate Retrofit Bottom Web Gap

Retrofit dimensions evaluated experimentally were chosen based on results of the computer simulations described in Section 3.1.3 and Appendix A.2 of this report, and on availability of structural steel shapes. Angle and plate sizes were L6x6x$^3/_4$ and PL18x8x$^3/_4$, respectively (see Figure 3.2).The angles were connected to the web, transverse connection plate (CP), and the backing plate with two fully-tensioned bolts on each leg (see Figure 3.3). A 9.5 mm ($^3/_8$ inch) thick shim plate was placed between the CP and the angle to eliminate the need for any chamfering or grinding of the edge of the angles. The back plate was installed on the fascia side of the girder, and was connected to the angles via four fully-tensioned bolts. The angles and back plate were removed every 250,000 cycles to allow for inspection of the web gap region and measurement of crack growth.

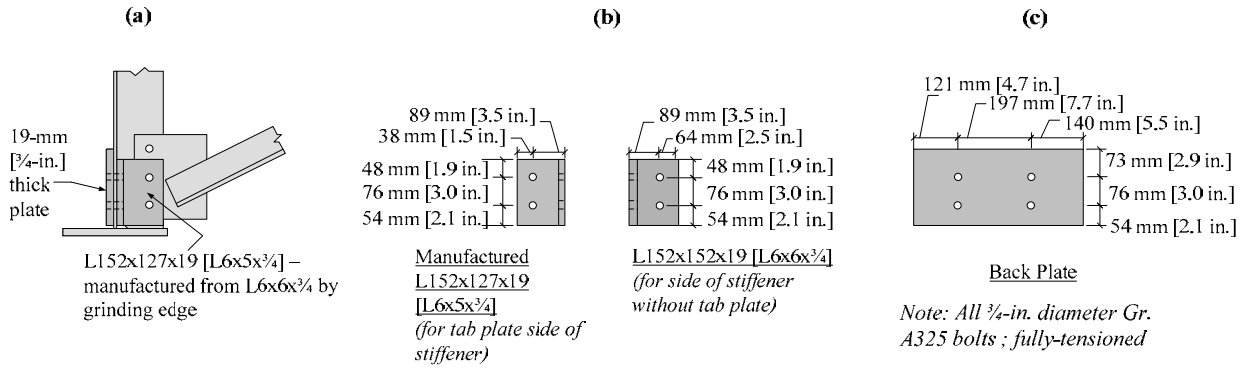

Figure 3.2: Schematic of elements used in the angles-with-plate repair

Figure 3.3: Angles-with-plate repair installed in the bottom web gap of the 2.8 m (9.3 ft) girder model

3.1.2 Physical Testing Performed on Bridge Model

The following discussion is a brief summary of the physical testing performed on the test bridge. Additional details may be found in Appendix A.3 and A.4.

The goal of evaluating the angles-with-plate retrofit in a scaled, multi-girder test bridge was to evaluate the effectiveness of the retrofit in a test that captured both in-plane bending effects and secondary stresses from distortion-induced fatigue. Therefore, a model was constructed that included three 9.1 m (30 ft) long girders connected with X-type cross frames at the two simple support locations and at midspan. A 127 mm (5 inch) thick concrete deck was cast in sections and was connected to the girders such that it would act compositely. All loads were applied through a 1,468 kN (330 kip) servo-controlled hydraulic actuator situated over a steel bearing plate centered on the bridge deck. A schematic of the test configuration, including girder dimensions, is shown in Figure 3.4.

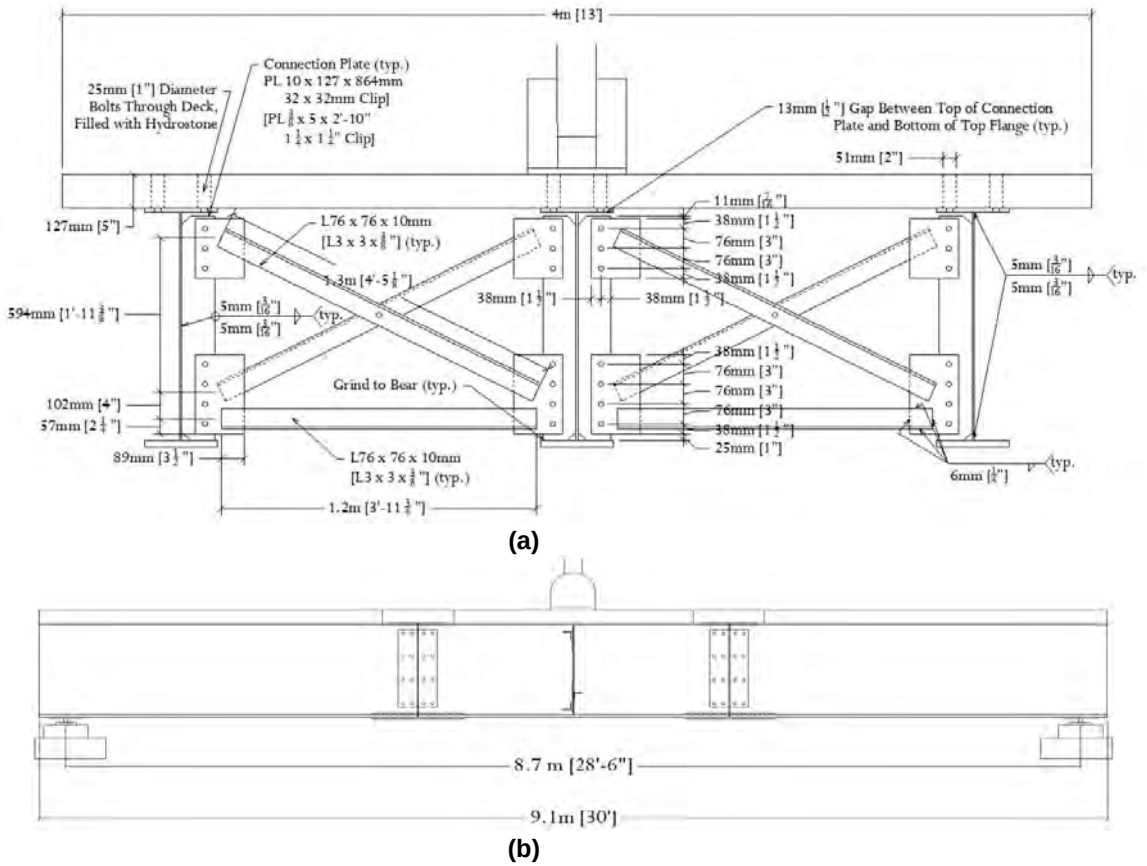

Figure 3.4: Dimensions and schematic of the bridge model

The bridge model was instrumented such that strain, vertical deflections, and lateral deflections could be measured through the test sequence. Additionally, load and displacement data were recorded from the actuator using the same data acquisition system that was used for all other sensors. Crack inspection was performed at regular intervals while the bridge was subjected to cyclic loading.

Fourteen test trials were performed on the bridge model, summarized in Table 3.2. For each loading protocol that was imposed on the bridge system, the two exterior girders (the north girder and the south girder) were considered to have been subjected to a single test trial. The center girder was not listed as undergoing a test trial, because the center girder did not experience any cracking throughout the test sequence (and was not expected to due to symmetric loading). Trial 1 consisted of an unretrofitted specimen in which cracking was allowed to initiate and propagate until a crack length of 24 mm (1 inch) was achieved. Trials 2, 3, 5, 6, and 7 were

indicative of the bridge with the exterior girders in the retrofitted condition (sometimes with the addition of crack stop holes), with each trial having a duration of 1.2 million cycles, with the exception of Trial 4. Trial 4 was the only trial in the retrofitted configuration that did not reach 1.2 million cycles, for reasons discussed further in Section 4.1.2 and Appendix A.3. Trials 2 to 6 utilized a non-stiffened version of the angles-with-plate retrofit (see Figure 3.5), while Trial 7 utilized a stiffened version of the angles-with-plate retrofit pictured in Figure 3.6.

Table 3.2: Specimen Test Trials for North (N) and South (S) Girders with Load Range

Trial	Specimen Description	Target Load Range
1N **1S**	Bare specimen – cycled to develop cracking in the bridge model	27-267 kN (6-60 kip)
2N **2S**	"Angles-with-plate" retrofit applied in top web gap	27-267 kN (6-60 kip)
3N **3S**	Same as Trials 2N and 2S: "Angles-with-plate" retrofit applied in top web gap	36-356 kN (8-80 kip)
4N **4S**	Small drilled holes with "angles-with-plate" applied in top web gap	44-445 kN (10-100 kip)
5N **5S**	Larger drilled hole with "angles-with-plate" retrofit applied in top web gap	44-445 kN (10-100 kip)
6N **6S**	Same as Trials 5N and 5S: Larger drilled hole with "angles-with-plate" retrofit applied in top web gap	53-534 kN (12-120 kip)
7N **7S**	Stiffened angles-with-plate retrofit applied in the top web gaps of exterior girders	53-534 kN (12-120 kip)

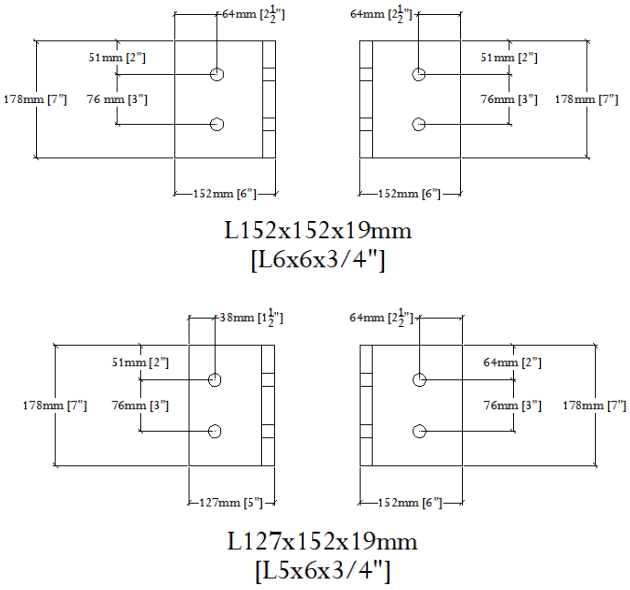

(a)

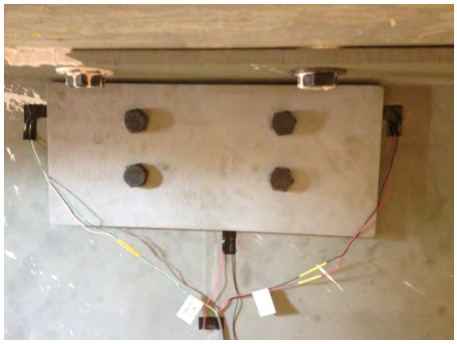

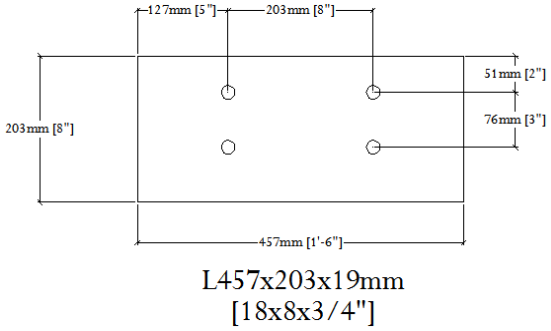

(b)

Figure 3.5: Angles-with-plate retrofit applied in Trials 2 to 6
(a) angles (b) back plate

Figure 3.6: Stiffened angles-with-plate retrofit applied to exterior girders in Trial 7

The load range applied to the bridge model was changed over the course of the testing sequence, as shown in Table 3.2, to thoroughly evaluate the performance of the angles-with-plate retrofit measure and its effectiveness at reducing the propensity to distortion-induced fatigue damage.

3.1.3 Computational Simulations for Girder Model Configuration

Computer models were created to resemble as closely as possible the girder-and-cross frame subassemblies tested in the companion experimental study. Given the interactions that exist between primary and secondary actions in a bridge, it is recognized that a complete bridge system provides a far superior platform to evaluate the efficacy of retrofit measures than girder subassemblies. The main advantage of using subassemblies is that experimental studies can be performed at a fraction of the cost of testing a complete bridge system. There is a similar advantage for computer models because smaller subassemblies allow areas of interest to be discretized with a greater number of elements.

Linear-elastic finite element (FE) models were created using eight-node brick elements (C3D8), each with 24 degrees of freedom. An appropriate level of mesh density was determined by performing analyses with various element sizes in the web gap region. The number of

elements in each model ranged between one and two million, depending on the retrofit measure that was modeled and the configuration of the fatigue cracks. Simulations were performed using the commercially-available finite element software, Abaqus (SIMULIA 2008).

The computer model was loaded with a single 222 kN (5 kip) force, applied to a WT section used to connect the cross frame members to the actuator, as in the physical model (Figure 3.7). This force corresponded to the maximum force applied to the physical models.

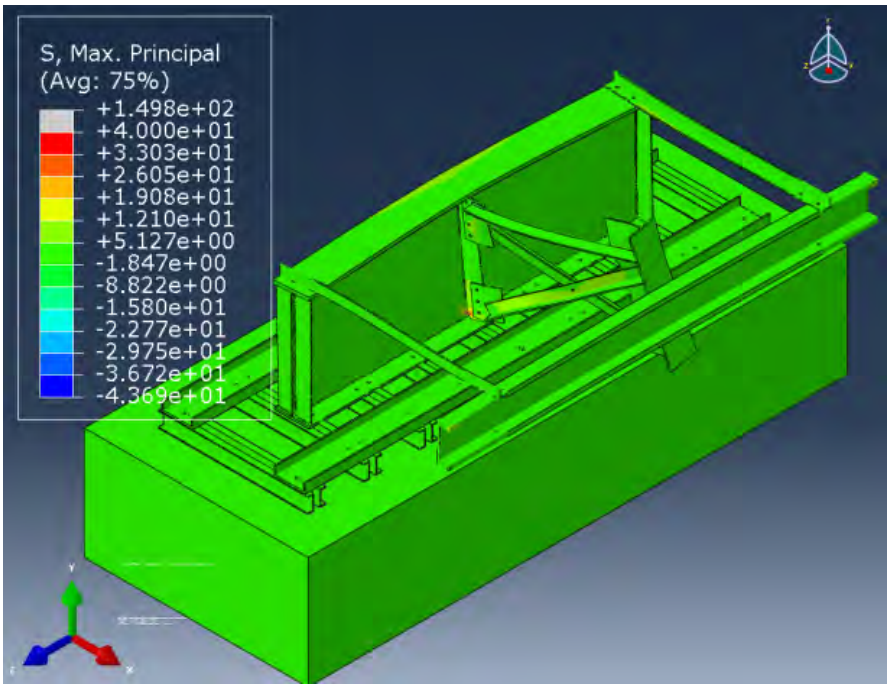

Figure 3.7: Overall view of finite element model corresponding to the physical test set-up

Computed stresses from different models were compared using a Hot Spot Stress (HSS) technique, described in detail in Appendix A.2. The adopted HSS technique was used to obtain a more reliable measure of stress demand in areas of the web gap region where there were large stress gradients, such as near welded or bolted connections and geometric discontinuities.

Figure 3.8 presents a comparison of the computed maximum principal stress demand in the web gap region and the physically-observed crack patterns noted in the experimental study for Specimens 1 and 2. It can readily be observed that the largest maximum principal stress demands in the model correlated very well with locations where cracks formed in the specimens. Therefore, maximum principal stresses were used as a measure of vulnerability to fatigue

damage because direct comparisons between computer simulation and experimental results showed that this was appropriate.

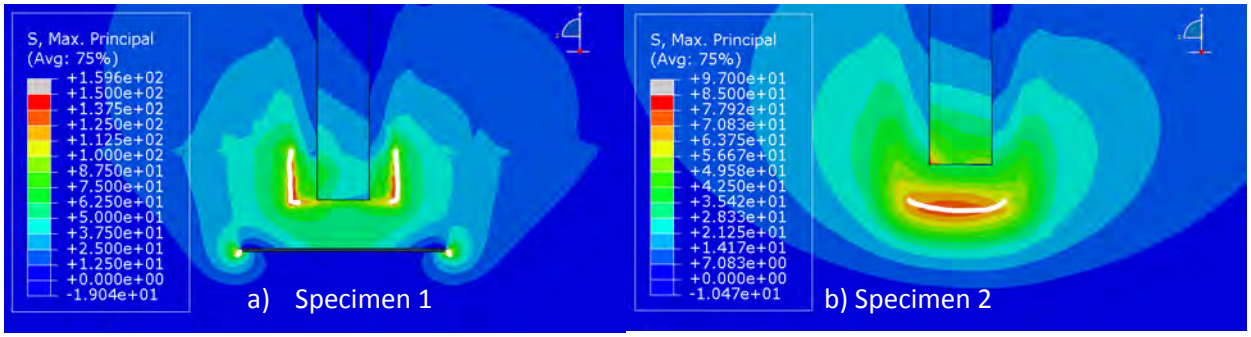

Figure 3.8: Observed crack patterns superimposed on the maximum principal stress contours from the simulation models for web gap regions of specimens 1 and 2 (Observed cracks shown as white lines). Circular shapes at the tips of the crack in (a) stem from the stress contours at those locations and are not to be confused with crack-arrest holes. Stress contour in (b) also corresponds to the configuration without crack-arrest holes.

3.1.4 Computational Simulations of Bridge Model

The three-girder, 9.1 m (30 ft) bridge model was modeled as faithfully as possible using the commercially-available finite element software Abaqus v.6.10 (SIMULIA 2008) Views of the finite element model are shown in Figure 3.9.

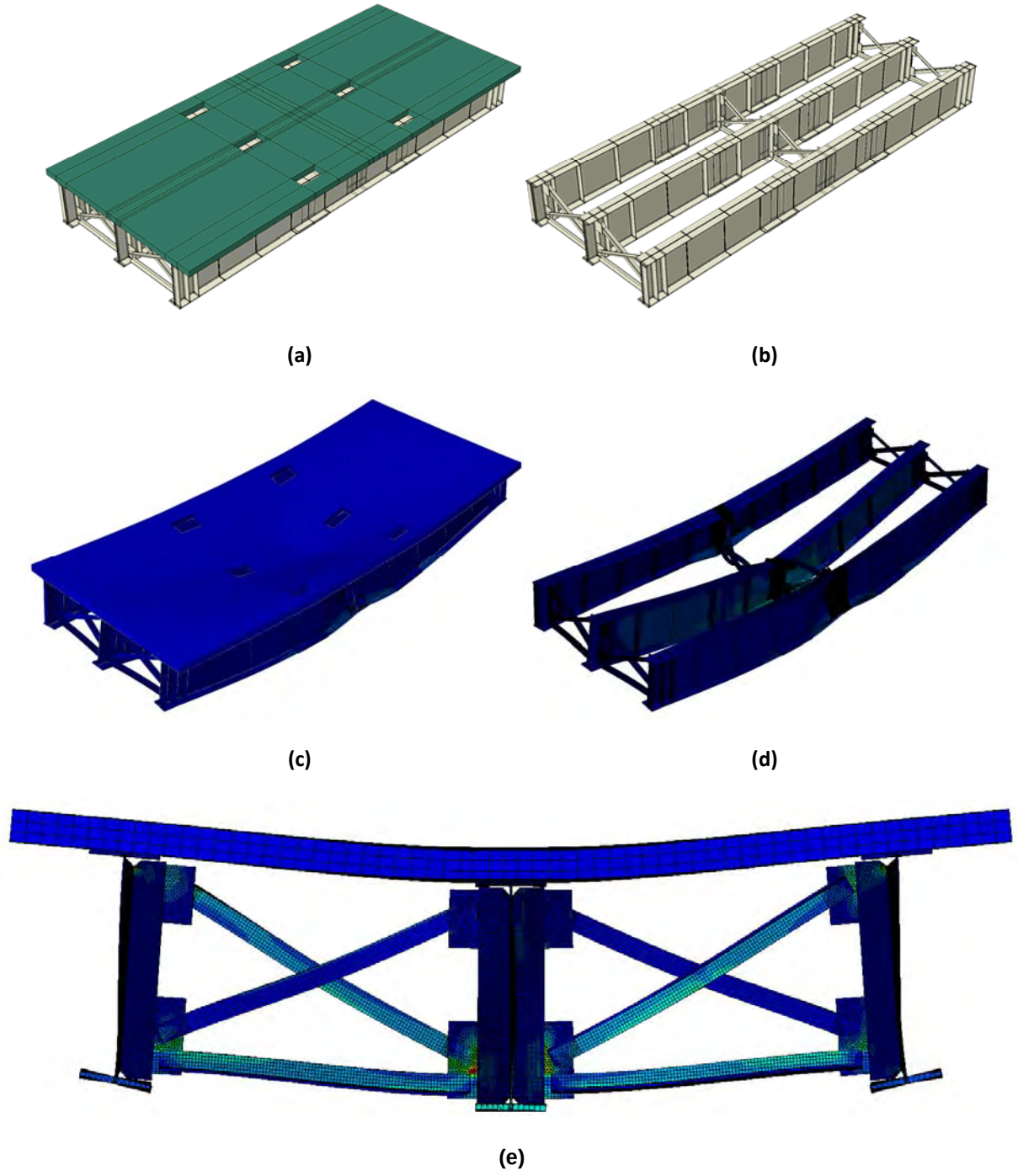

Figure 3.9: Views of the finite element model
(a) Overall model with concrete deck, (b) overall model without concrete deck, (c) deflected model with concrete deck, deflection scale=425, (d) deflected model without concrete deck, deflection scale=425, and (e) deflected section cut at mid-span, deflection scale=100.

All bridge components were constructed in Abaqus v.6.10 (SIMULIA 2008) using three dimensional elements, including the welds, cross-frames, stiffeners, and deck. Each model contained approximately 3 million elements and 10 million degrees of freedom. A highly dense mesh was utilized within the web gap region while other locations within the bridge contained a less dense mesh. Steel and concrete were modeled as linear-elastic materials where the modulus of elasticity for each was taken as 200 GPa (29,000 ksi) and 24.9 GPa (3,605 ksi), respectively. Poisson's ratio for steel and concrete was taken as 0.3 and 0.2, respectively.

Forty-five finite element models were constructed and analyzed for various configurations of the baseline test bridge geometry. Models included cracked and uncracked conditions in the top web gap of the exterior (north and south) girders. Cracked models included either a horseshoe-shaped crack around the connection-plate-to-web weld or a longitudinal crack along the web-to-flange weld. A modeling test matrix is shown in Table 3.3.

A single-point hot spot stress (HSS) procedure was used as the basis for stress comparisons in which stresses were extracted at a set distance (half the web thickness, 3 mm [$^1/_8$ inch]) from the discontinuity, either a weld or crack. This procedure was found to be less sensitive to mesh density than extracting maximum stress from the models (Adams 2009).

Several variations of the angles-with-back plate retrofit were explored, in which the thickness of the angle and plate elements were varied (with retrofit thickness–to–web thickness ratios of 2.0 and 3.0), and one case in which the angles were modified to include internal stiffeners to reflect the retrofit measure used in Test Trial 7 of the physical test. Schematics of the retrofit measures studied in the computational simulations performed for the model bridge configuration are shown in Figure 3.10.

Table 3.3: Finite Element Modeling Matrix for Cracks around Connection Plate-to-Web Weld

	Model Description / Crack Length	No Crack	25 mm (1 in.)	38 mm (1-1/2 in.)	51 mm (2 in.)	64 mm (2-1/2 in.)	76 mm (3 in.)	101 mm (4 in.)	203 mm (8 in.)
Connection Plate-to-Web Cracks	Unretrofitted condition	X	X	X	X	X	X	X	X
	Reduced deck stiffness with unretrofitted condition				X				
	Broken cross-frame		X						
	Angles-with-plate repair with 19 mm (3/4 in.) thicknesses		X	X	X	X	X		
	Stiffened angles-with-plate repair with 19 mm (3/4 in.) thicknesses		X	X	X	X	X		
	Angles-with-plate repair with 13 mm (1/2 in.) thicknesses		X	X	X	X	X		
	Traditional angles repair connected to flange with 19 mm (3/4 in.) thickness		X	X	X	X	X		
	Back-up stiffener repair placed on fascia side		X	X	X	X	X		
Flange-to-Web Cracks	Unretrofitted condition		X		X		X	X	X
	Angles-with-plate repair with 19 mm (3/4 in.) thicknesses		X		X		X	X	X

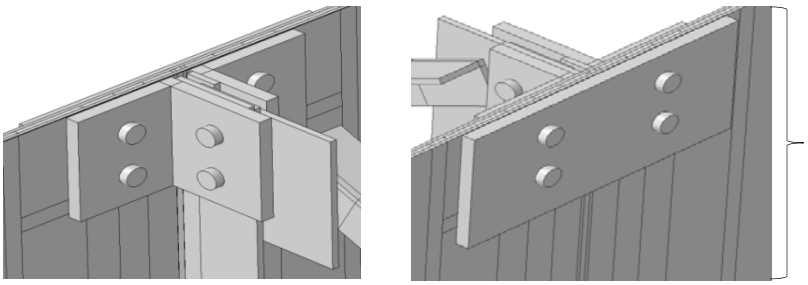

Angles:
L152x152 mm (L6x6 in.)
L127x152 mm (L5x6 in.)

Backing Plate:
457x457 mm (18x8 in.)

(a)

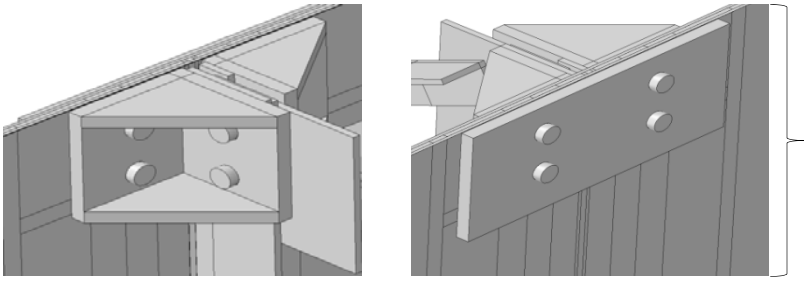

Angles:
L152x152 mm (L6x6 in.)
L127x152 mm (L5x6 in.)

Stiffeners:
133x133 mm (5.25x5.25 in.)
108x133 mm (4.25x5.25 in.)

Backing Plate:
457x457 mm (18x8 in.)

(b)

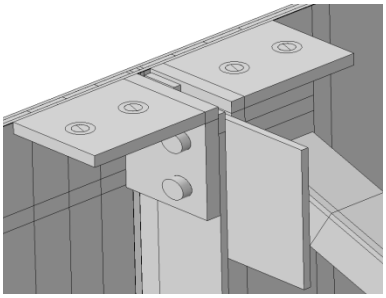

Angles:
L179x179mm (L7x7 in.)

(c)

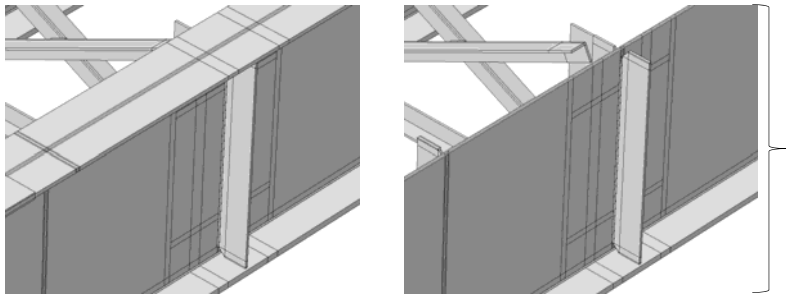

Back-up Stiffener:
9.5x127x876 mm (3/8x5x34-1/2 in.)
with 32x32 mm (1-1/4x1-1/4 in.) clip

(d)

Figure 3.10: Views of various retrofits examined in the finite element models (a) angles-with-plate retrofit measure; (b) stiffened angles-with-plate retrofit; (c) positive attachment between transverse connection stiffener and top flange retrofit; and (d) full depth back-up stiffener bearing on top and bottom flanges.

3.2 Development of Fiber-Reinforced Polymer Retrofit Measures

A series of fiber-reinforced polymer (FRP) retrofit measures were developed and tested under TPF-5(189) to evaluate the potential of this previously unused material for the repair of fatigue damage:

- Initial testing was performed on small scale bending-type and tension-type fatigue specimens to determine merit of the concept and to identify and address challenges with materials, application methods, and achieving adequate bond. (Sections 3.2.1 and 3.2.2);
- A series of physical tests were performed within the girder model configuration in which two primary techniques were developed and tested (Section 3.2.3):
  - A composite block retrofit measure
  - A variation of the angles-with-plate retrofit that included a layer of carbon fiber reinforced polymer (CFRP) material sandwiched between the steel girder and the steel retrofit elements
- A series of computational simulations complementing the above physical investigations (Section 3.2.4).

A brief summary of the methodologies for each of these aspects of TPF-5(189) are presented in the following sections, with references made to Appendices B.1 to B.6.

3.2.1 Physical Testing Performed on Tensile Fatigue Specimens

A series of fatigue tests were performed on small-scale steel tension specimens to determine the effectiveness of CFRP overlays to repair existing fatigue damage in steel plates. Fifteen steel plate specimens were repaired with CFRP overlays of various thicknesses to evaluate the effect of the stiffness ratio, *SR*, on fatigue crack propagation and effective stress range. The stiffness ratio, *SR*, was defined as the product of the modulus of elasticity and thickness of the CFRP divided by the product of the modulus of elasticity and thickness of the steel. This aspect of the study aimed to identify relationships between the stiffness of CFRP overlays and steel substrate such that future CFRP repairs could be proportioned to effectively slow or halt crack propagation in the steel substrate.

The steel specimen type used in this portion of the study is shown in Figure 3.11 (dimensions for the 6.4 mm [$^1/_4$-inch] thick specimen were slightly different, and can be found in Appendix B.1, along with other detailed information regarding this portion of the study).

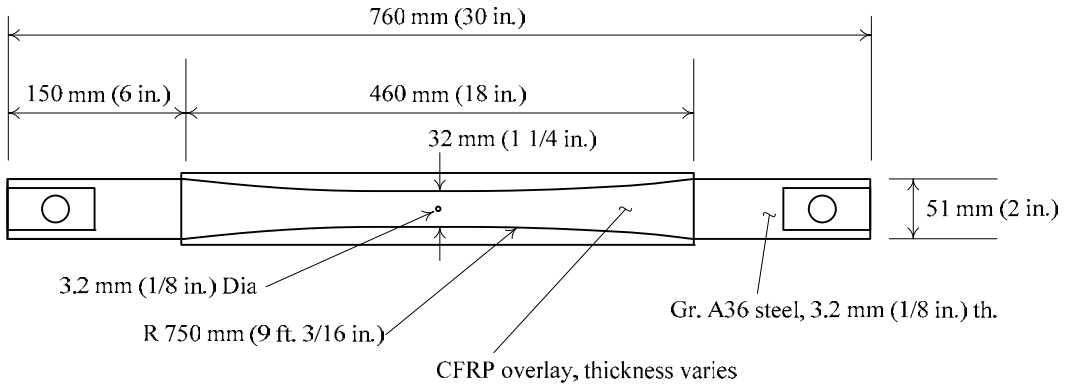

Figure 3.11: Tension specimen dimensions (for a 3.2 mm [$^1/_8$ inch] thick specimen)

Fatigue cracks were propagated on each side of the drilled and reamed hole at the center of the specimen, shown in Figure 3.11, until either of the cracks reached a length of approximately 7 mm (0.3 inch). After the initial crack length of 7 mm (0.3 inch) was reached, each specimen was repaired using CFRP overlays.

Two parameters were varied in this study that had an effect upon the stiffness ratio between the CFRP and the steel: t_{CFRP} and the thickness of the steel plate, t_s. Testing was conducted at stress ranges of 166 MPa (24 ksi), 221 MPa (32 ksi) and 263 MPa (38 ksi), to evaluate effect of the *SR* at various stress ranges. The test matrix is shown in Table 3.4.

Table 3.4: Specimen Test Matrix

Specimen Designation	Specimen Thickness mm (inch)	CFRP Overlay Thickness mm (inch)	Stress Range MPa (ksi)	Fatigue Crack Propagation Life
F15	3 ($^1/_8$)	1.6 ($^1/_{16}$)	263 (38)	18,900
F3	3 ($^1/_8$)	1.6 ($^1/_{16}$)	221 (32)	60,000
F6	3 ($^1/_8$)	1.6 ($^1/_{16}$)	166 (24)	340,700
Pick12	3 ($^1/_8$)	2.4 ($^3/_{32}$)	221 (32)	271,100
Pick11	3 ($^1/_8$)	3.2 ($^1/_8$)	263 (38)	95,100
F14	3 ($^1/_8$)	3.2 ($^1/_8$)	221 (32)	313,050
F2	3 ($^1/_8$)	3.2 ($^1/_8$)	166 (24)	1,450,095
Pick10	3 ($^1/_8$)	6.4 ($^1/_4$)	263 (38)	282,550
Pick13	3 ($^1/_8$)	6.4 ($^1/_4$)	221 (32)	Run-Out
Pick7	3 ($^1/_8$)	6.4 ($^1/_4$)	166 (24)	Run-Out
F27	3 ($^1/_8$)	12.8 ($^1/_2$)	221 (32)	Run-Out
F4-25	6 ($^1/_4$)	1.6 ($^1/_{16}$)	221 (32)	15,600
F4-21	6 ($^1/_4$)	3.2 ($^1/_8$)	221 (32)	160,150
F4-23	6 ($^1/_4$)	6.4 ($^1/_4$)	221 (32)	571,650
F4-20	6 ($^1/_4$)	12.8 ($^1/_2$)	221 (32)	Run-Out

The multi-layered CFRP overlays were pre-fabricated and attached to the steel specimens after a fatigue crack had been propagated to a pre-determined length. To develop adequate bond, the steel surface was prepared by a process of abrading and cleaning before the overlays were applied. After the CFRP bond layer had been allowed to cure, the retrofitted specimen was subjected to fatigue loading in an MTS closed-loop servo-controlled loading system.

3.2.2 Physical Testing Performed on In-Plane Bending Fatigue Specimens

A series of tests were performed on small-scale bending-type fatigue specimens to determine viability of using FRP materials as a fatigue retrofit under significant bending demands, producing both peel- and shear- type stresses in the bond layer between the CFRP and steel (as would be the case in a web gap region loaded under distortion-induced fatigue). The detail chosen was a welded cover plate – chosen because of the severity of the detail (Category E or E', depending upon plate thicknesses), and because of the simplicity of the specimen and resulting stresses. The specimens used for this portion of the project are shown in Figure 3.12. A

major goal of this testing sequence was to refine procedures for bonding the FRP material and the steel substrate.

The composite ‘doubler’ elements developed to repair this connection detail were comprised of CFRP material, and are shown in a schematic in Figure 3.12. The doubler elements were bonded to the steel substrate using Hysol™ resin; bond layers of varying thicknesses [0.3 mm ($^1/_{32}$ inch) to 6.4 mm (¼ inch thick)] were examined as part of this investigation. Additionally, the presence of a fibrous layer within the bond layer (composed of polyester breather cloth) and the effect of including a ‘resin pool’ beyond the extents of the doubler footprint were considered within the test matrix. The composition of the CFRP doubler was also varied: doubler elements were created using sheet-type carbon fiber placed in layers, and doublers were also created using chopped-fibers, representative of a spray-on type of CFRP mix. Specimens created using chopped fibers were investigated due to their potential ease-of-application in the field, and their capability to be easily molded to the needed geometry. The test matrix is shown in Table 3.5.

Specimens were tested in three-point bending after the pre-fabricated CFRP doubler elements were bonded to the steel specimens and the bond was permitted to cure. Each assembly was subjected to cyclic loading until crack initiation was observed in the steel substrate or run-out was achieved. The applied load range was such that a nominal bending stress of 138 ksi (20 ksi) was applied at the toe of the transverse welds at the termination of the cover plate. Each time debonding of an overlay was observed, the overlay was removed and the weld was inspected for the presence of fatigue cracks. If fatigue cracks were not observed, the overlay was rebonded and fatigue testing resumed. Further details regarding the test design and parameters can be found in Appendix B.2 and B.3.

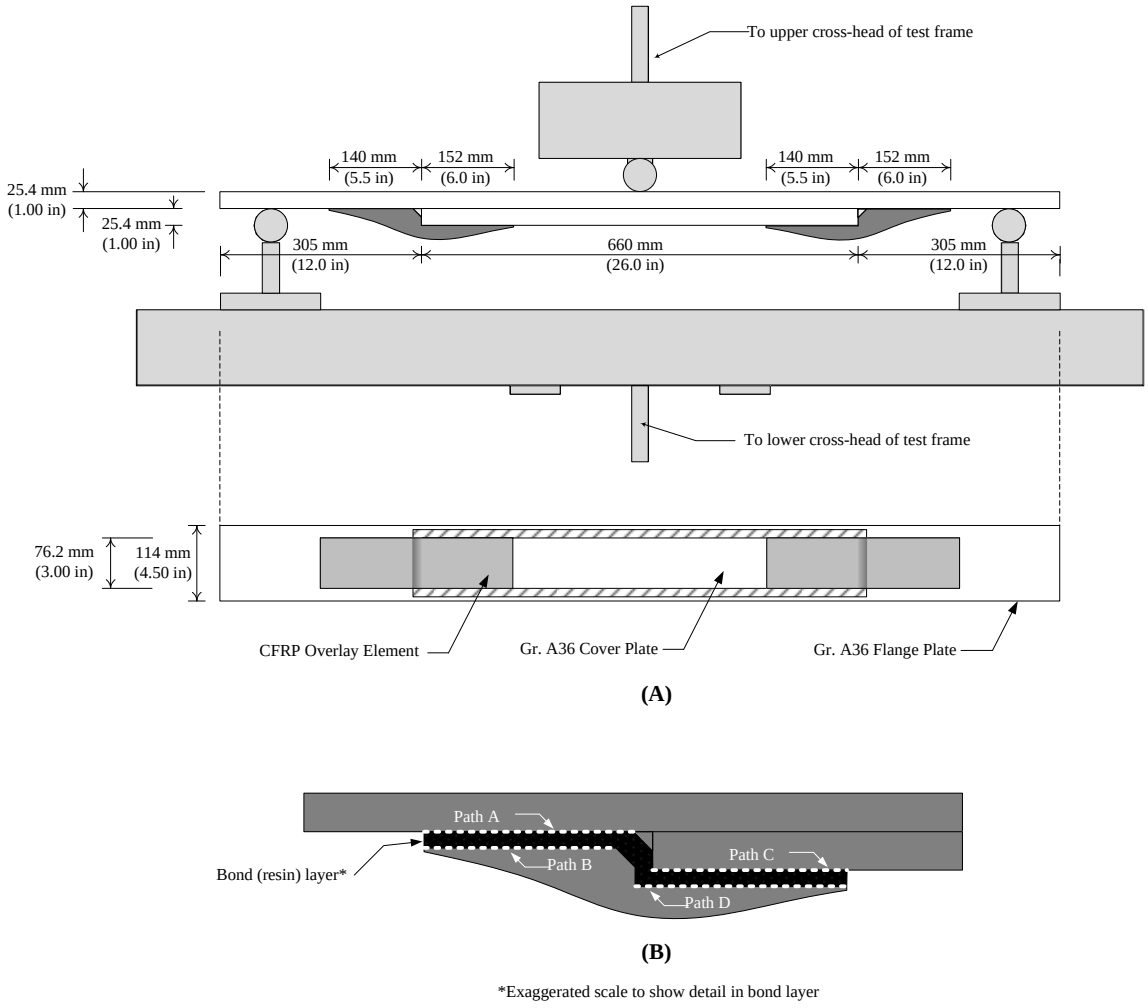

Figure 3.12: View of bending-type specimens with carbon fiber reinforced polymer overlay elements

Table 3.5: Fatigue Testing Program and Results for Carbon Fiber Reinforced Polymer-Stiffened Specimens

Specimen	Test Designation	Number of Cycles to Bond Failure	Breather Cloth	Resin Pool	Resin Layer Thickness mm (in.)
TRI 02	C0030-01	275,000	N	N	0.8 ($^1/_{32}$)
TRI 02	C0030-02	900,000	N	N	0.8 ($^1/_{32}$)
TRI 04	C0125-01	529,800	N	N	3.2 ($^1/_8$)
TRI 04	C0125-02	255,750	N	N	3.2 ($^1/_8$)
TRI 04	C0125-03	134,150	N	N	3.2 ($^1/_8$)
TRI 04	C0125-04	71,150	N	N	3.2 ($^1/_8$)
TRI 04	C0125-05	204,500	N	N	3.2 ($^1/_8$)
TRI 04	C0125-06	1,125,300 *	N	N	3.2 ($^1/_8$)
TRI 04	CP0125-01	1,060,950 *	N	Y	3.2 ($^1/_8$)
TRI 04	CP0125-02	722,000 *	N	Y	3.2 ($^1/_8$)
TRI 06	CP0065-01	279,750	N	Y	1.6 ($^1/_{16}$)
TRI 06	CP0065-02	283,900	N	Y	1.6 ($^1/_{16}$)
TRI 06	CP0065-03	239,250	N	Y	1.6 ($^1/_{16}$)
TRI 06	CP0065-04	956,606	N	Y	1.6 ($^1/_{16}$)
TRI 06	CP0065-05	398,596	N	Y	1.6 ($^1/_{16}$)
TRI 05	CPB0250-01	1,205,315	Y	Y	6.4 ($^1/_4$)
TRI 05	CPB0250-02	1,634,756 *	Y	Y	6.4 ($^1/_4$)
TRI 07	CPB0125-01	1,725,900 *	Y	Y	3.2 ($^1/_8$)
TRI 07	CPB0125-02	1,725,900 *	Y	Y	3.2 ($^1/_8$)
TRI 07	CPB0125-03	1,564,300 *	Y	Y	3.2 ($^1/_8$)
TRI 07	CPB0125-04	1,564,300 *	Y	Y	3.1 ($^1/_8$)

3.2.3 Physical Testing Performed on Girder Models

The following sections describe two different FRP retrofit measures tested using the 2.7 m (9.3 ft) girder model configuration. The first FRP retrofit measure described is a composite block that was cast in the web gap region of a test specimen (described in Part 3.2.3.1 in brief, and Appendix B.4 in greater detail). The second FRP retrofit described is a variation of the angles-with-plate technique, adapted for deep web cracks in the form of a sandwich-type composite (described in Part 3.2.3.2 in brief and Appendix B.6 in greater detail).

3.2.3.1 Composite Block Retrofit

The experimental program described in this section was carried out to evaluate the performance of a fiberglass reinforced polymer (FRP) composite block as a method of repairing distortion-induced fatigue damage in a girder web gap region. This study included a physical test

of a FRP composite block applied to a 2.8 m (9.3 ft) long girder model subjected to distortion-induced fatigue, which is discussed in more detail in Appendix B.4 of this report.

The girder model used was similar to the one described in Section 3.1.1 of this report. The girder subassembly was tested under a cyclic tensile force (the force was applied upwards at the WT- connected to the cross-frame) ranging from 2.2 kN (0.5 kip) to 25.3 kN (5.7 kip). The test was divided into two trials; Test Trial 1 was performed on the girder subassembly without any applied retrofit measure, followed by Test Trial 2 in which composite block retrofit was applied to the girder subassembly.

In Trial 1, a web-to-connection plate crack was initiated and propagated to a length of 57 mm (2 ¼-in.), at which point the composite block retrofit was applied to the girder. The cracking presented as a "horseshoe-shaped" crack, forming around the connection plate-to-web weld. Before the composite block retrofit was applied, the girder subassembly was inspected every one thousand cycles using UV light and dye penetrant. Once the intended crack length was achieved, the composite block retrofit was cast on the interior face of the girder, on both sides of the connection plate (Figure 3.13).

The composite was comprised of West System™ two-part epoxy (West System™ 105 Epoxy Resin and West System™ 206 Slow Hardener) and conventional mat fiberglass. Wooden molds were firmly held in position through use of 19 mm ($^3/_4$ inch) threaded rods, which remained in-place during the fatigue testing, and provided additional connectivity between the composite and the steel. No mechanical connection between the girder flange and the composite block was made, as the intent of this technique was to repair the web gap region without interfering with the flange.

After the composite retrofit was installed, the girder subassembly was tested for an additional 1.2 million cycles (Trial 2). At the end of Trial 2, the composite blocks were removed, and the girder subassembly was then inspected for any possible crack growth.

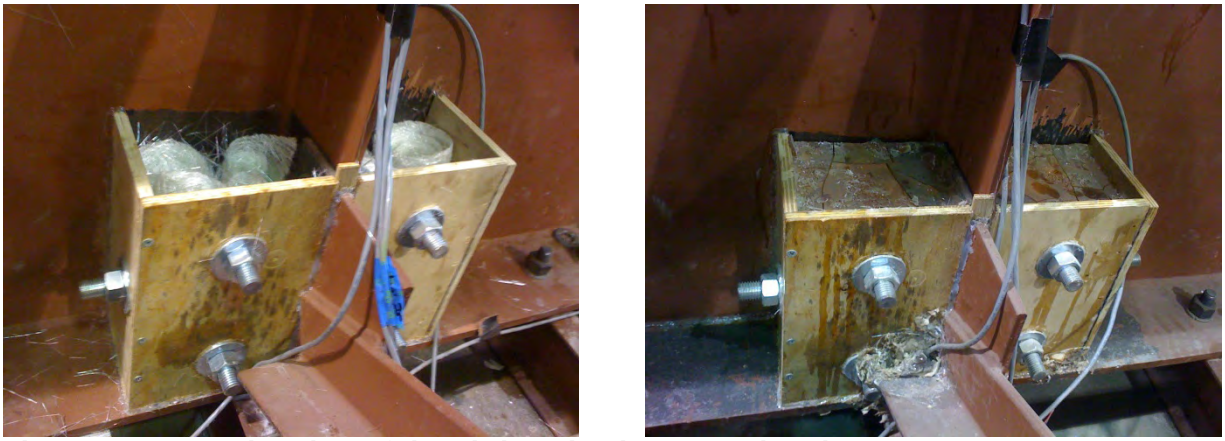

Figure 3.13: Interior view of the girder: a) Prior to casting the West System™ two-part epoxy. b) View of the cured composite blocks.

3.2.3.2 Sheet-type CFRP + Steel Repair

A variation of the angles-with-plate retrofit was examined in a 2.7 m (9.3 ft) long girder model with severe cracking in the web of the girder, in which a version of the angles-with-plate retrofit was installed both with and without a CFRP layer between the steel retrofit elements and the girder. This retrofit is described in greater detail in Appendix B.6 of this report, and is shown in Figure 3.14 and 3.15.

Two test trials were performed in this test series that included: (1) a version of the steel-only angles-with-plate retrofit and (2) the angles-with-plate retrofit including a layer of CFRP between the girder and the steel retrofit elements. In each of the two trials, the specimen was subjected to 1.2 million cycles. In both cases, the retrofit measures were applied over a very severe distortion-induced fatigue crack that had been allowed to propagate to approximately 50% of the web depth.

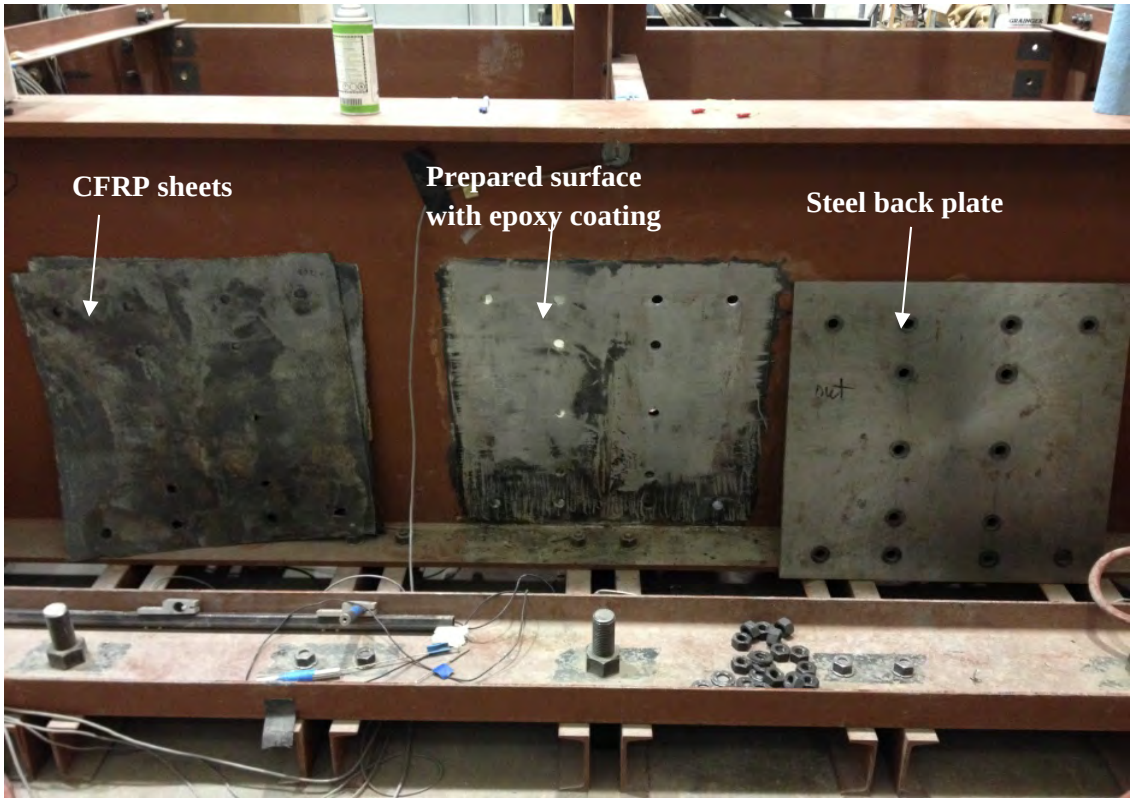

Figure 3.14: View of the exterior face of the girder web before application of the steel backing plate with CFRP sheets bonded to the girder and sandwiched between the girder and plate

Figure 3.15: Trial 2: view of the interior face of the girder's web before application of the angles-with-plate-with-CFRP retrofit measure

3.2.4 Computational Simulations

Computational simulations were performed to augment and inform the development of FRP retrofits for distortion-induced fatigue. Simulations were performed using Abaqus to better understand the mechanisms of failure and the effects of various parameters on stress demand with and without FRP retrofit measures (SIMULIA 2008). Short descriptions of the modeling approach are provided here, with references made to the more detailed discussions in Appendix B.

3.2.4.1Tensile Fatigue Specimens

A series of computational simulations were performed to accompany the physical testing described in Section 3.2.1 of this report. The FE models were used to complement the physical tests performed on the tensile fatigue specimens overlaid with CFRP doublers, to determine the effects of bond layer thickness and CFRP overlay thickness of the reduction in HSS demand. FE models were developed using linear-elastic materials, and meshes were assembled using eight-node brick elements. Further description regarding the computational simulation methodology for this portion of the overall study can be found in Appendix B.1.

3.2.4.2 In-Plane Bending Fatigue Specimens

A series of computational simulations were performed to accompany the physical testing described in Section 3.2.2. The analyses were performed to characterize the stress field in the region surrounding the weld toe and to quantify the effects of the characteristics of the overlay on the stress demand at the weld toe. Two-dimensional and three-dimensional finite element models were created using Abaqus v6.8, using linear-elastic materials for the steel and composite materials (SIMULIA 2008). The models were used to evaluate the effect of the following parameters on the state of stress at the fatigue-susceptible detail:

(a) CFRP overlay shape,
(b) Presence of a void in the CFRP overlay near the fatigue detail,
(c) CFRP overlay stiffness, and
(d) Thickness of the bond layer between the steel and CFRP overlay.

The modeling methodology used in this portion of the study is described in detail in Appendix B.2 and B.3.

3.2.4.3 FRP Retrofit Measures Modeled with the Girder Model Configuration

3.2.4.3.1 Composite block retrofit measure

A finite element model was created to examine the effect of adding a composite block to the web gap region in a girder subjected to distortion-induced fatigue. The composite block was modeled as an added component of a cracked girder model. The block was assigned dimensions of 114 x 114 x 127 mm (4.5 x 4.5 x5.0 in.) and was modeled as attached to both sides of the connection plate, the adjacent flange, and the web in the bottom web gap of a girder segment through use of tie constraints. An upward load of 22.2 kN (5 kip) was applied to the actuator in the model to simulate the loading applied in the experimental tests. Because the block was tied to all contact surfaces, the results from this model should be viewed as one extreme end of possible behavior (i.e., it is plausible that a majority of bond could be lost between contact surfaces during physical testing). Further details regarding this can be found in Appendix B.4.

3.2.4.3.2 Sheet-type CFRP + Steel Repair

The performance of three different repair methods for girders with large cracks caused by distortion-induced fatigue was investigated through use of computational simulations. Effectiveness of the repair methods was quantified on the basis of the computed reduction in stress demand with respect to companion models of unrepaired girders with a simulated crack. The three repair methods evaluated were: (1) drilling crack-stop holes of varying diameter at the crack tips, (2) attaching bolted splice plates over the full depth of the girder (including drilled crack-stop holes at the crack tips) as shown in Figure 3.16, and (3) attaching a repair assemblage consisting of bonded CRFP overlays reinforced with bolted steel cover plates (including drilled crack-stop holes at the crack tips) as shown in Figure. For the third repair type, two different crack lengths were considered: $^1/_8$ the depth of the web and ¼ the depth of the web. The steel plate elements were modeled separately from the CFRP sheet, which was also modeled separately from the resin layer.

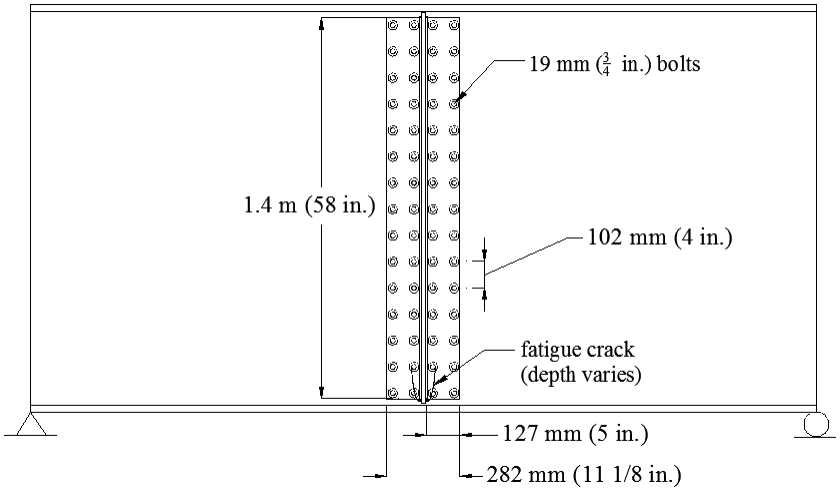

Figure 3.16: Full-depth splice plate fatigue damage repair

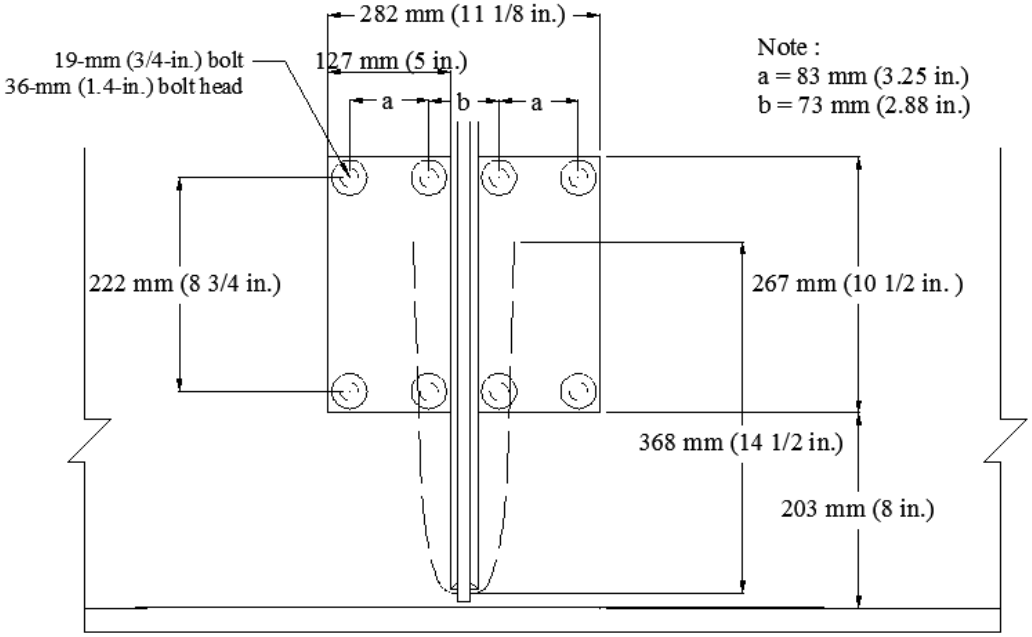

Figure 3.17: Repair dimensions for crack length equal to ¼ of the web depth

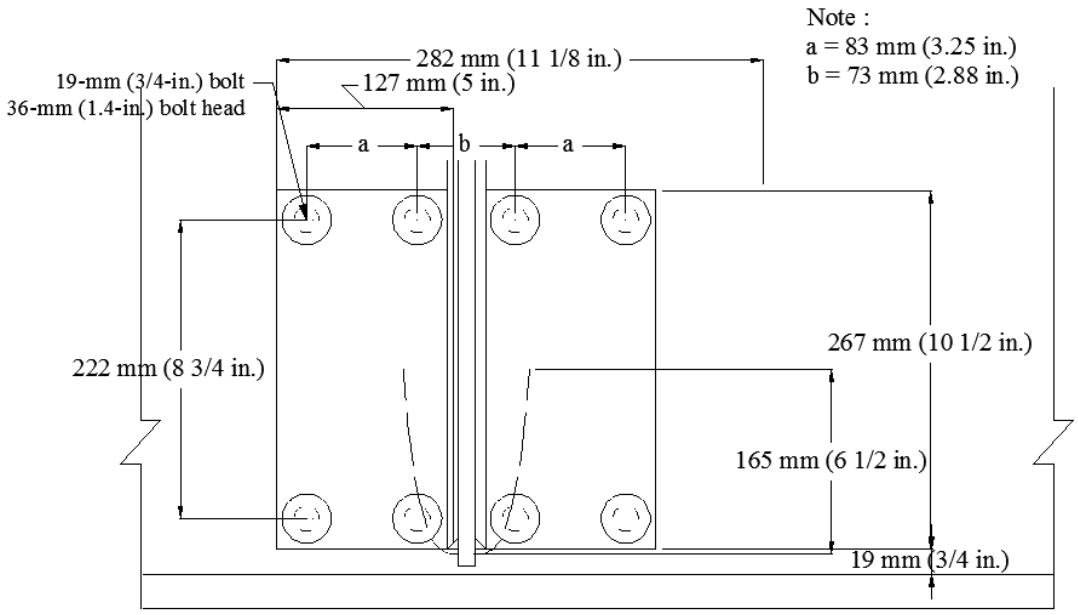

Figure 3.18: Repair dimensions for crack length equal to $^1/_8$ of the web depth

While these repairs were not identical to the version of the sandwich-type composite repair for deep cracks tested in the girder model test set-up (described in Section 3.2.3.2), they are still useful in determining the validity and usefulness of the general repair approach. Detailed discussion of the simulation techniques utilized in this portion of the study can be found in Appendix B.5.

3.3 Development of PICK Technology

A technique, termed Piezoelectric Impact Compressive Kinetics (PICK), was developed under TPF-5(189). A brief summary of the methods used during the development are described in the following, while detailed descriptions have been provided in Appendix C.

Development and testing of the PICK technology included:

- Developing the PICK tool and creating a prototype device
- Performing finite element analyses of treated crack-arrest holes in steel to validate the approach used
- Performing a series of measurements to gage effectiveness of the PICK technique (retained expansion, hardness, grain size analysis) and performing fatigue testing of untreated and treated tensile specimens.

3.3.1 Analytical Validation of Approach

First, the concept of treating a crack-arrest hole in a steel element through a cold-expansion process was explored through an analytical study. A series of 2D and 3D finite elements were created of a plate-type specimen with a hole at its midpoint. Two groups of models were created: one set utilized nonlinear material properties for Aluminum, and the other set utilized nonlinear material properties for mild steel. Both model groups were subjected to various levels of cold-expansion of the hole in the plate: 3%, 4%, 5%, and 6%. Previous research has shown that an optimum level of cold expansion of a fastener hole *in aluminum* using presently-accepted cold expansion techniques is approximately 4% larger than the original hole size. Therefore, the aim of the study was to determine if similar levels of residual compressive stresses could be obtained through cold-expansion of steel. This aspect of the PICK development is discussed more in Appendix C.1 of this report.

3.3.2 Development of PICK Technology and Testing

Next, the PICK device was developed and tested. The PICK tool was designed to apply a compressive force to an aluminum plug pressed into a drilled hole in a steel specimen. Poisson's effect causes the aluminum plug to expand in the radial direction, expanding the diameter of the hole in the specimen and focusing ultrasonic vibration into the steel specimen. A schematic of the PICK device is shown in Figure 3.19.

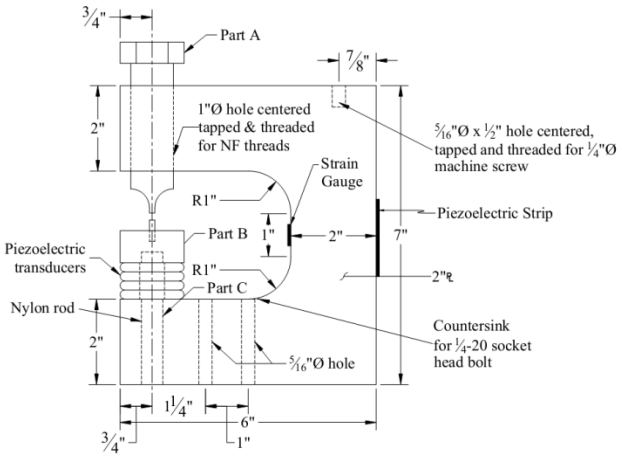

Figure 3.19: PICK tool schematic

The PICK tool was bench-mounted, with its major components being a C-shaped base, a threaded bolt, piezoelectric elements, and a round load-transfer plate. The tool was machined from 4140 annealed steel with yield strength of 412 MPa (60 ksi). The end of the bolt was machined to form a 3.2 mm ($^1/_8$ inch) diameter tip; force was applied to the plug by tightening the bolt at the top of the tool, thereby pressing the tip into the aluminum plug. Underneath the fatigue specimen was a round, load-transfer plate, which was machined to fit on top of a nylon rod and fit tight with the top of the piezoelectric stack beneath it. A hardened steel rod with a tip also machined to a 3.2 mm ($^1/_8$ inch) diameter was pressed into the top of the round load-transfer plate and completed the load path through the aluminum plug. When power was supplied to the piezoelectric element stack, they expanded in the vertical sense (with reference to Figure 3.19) at an adjustable ultrasonic frequency. The compression supplied to the aluminum plug (which was in turn fit-tight in the hole in the steel specimen) therefore produced compressive residual stresses in the steel, and also was expected to cold-work the hole surface through its repeated impact against the hole. Further details regarding the PICK tool development can be found in Appendix C.2 of this report.

Performance of the PICK tool was measured through the following means: fatigue testing, measuring levels of retained expansion, metallurgical investigation, hardness testing, and neutron diffraction measurements to quantify residual stresses.

3.3.2.1 Fatigue Testing

The fatigue testing program consisted of fifteen tensile fatigue specimens fabricated using Gr. A36 steel. The specimens were manufactured using 3.2 mm ($^1/_8$ inch) thick steel bar with a reduced cross-section at the center, as shown in Figure 3.20. A hole with a diameter of 3.2 mm ($^1/_8$ inch) was drilled and reamed at the center of each specimen at the point of minimum width. The expectation was that cracking would initiate at the location of the hole and would propagate in a direction perpendicular to the longitudinal axis of the specimen. The ends of the specimen were reinforced to prevent a localized failure in the region where the specimen interfaced with the grips of the testing machine.

Of the 15 specimens tested in fatigue, five received no treatment, four received “pressure-only” treatment (applied by tightening the PICK tool over the aluminum plug inserted in the steel

specimen, but not applying the ultrasonics), and six received full PICK treatment, which included the combination of pressure and ultrasonic treatment.

The pressure-only and PICK treatments were applied to the specimens through an aluminum plug inserted into the 3.2 mm ($^1/_8$ inch) diameter hole. The aluminum plugs were fabricated from 6061-T6 aluminum dowel stock having a slightly larger diameter than the hole drilled in the steel specimens. Each plug was also fabricated such that it was slightly longer than the thickness of the steel specimens.

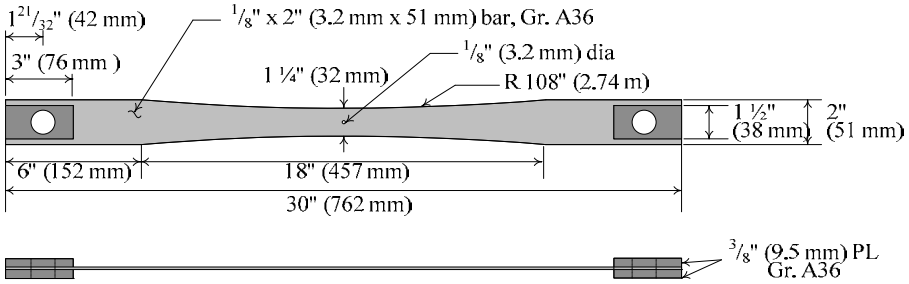

Figure 3.20: Fatigue specimen dimensions for PICK treatment

After treatment, all fatigue specimens were tested under tensile cyclic loading using an MTS universal testing machine. The frequency of the cyclic load was approximately 2 Hz, and the stress range was 32 ksi (221 MPa), with 2 ksi (14 MPa) being the lower limit and 34 ksi (234 MPa) being the upper limit.

3.3.2.2 Retained Expansion Measurements

Retained expansion (*RE*) is an important parameter that has been commonly used in prior research to measure the effectiveness of cold-expansion. Retained expansion is defined as the change in radius of an expanded hole, expressed as a percentage of the initial radius (Equation 3.1).

$$RE = \left(\frac{R_{final} - R_{initial}}{R_{initial}} \times 100 \right)\% \qquad \textbf{Equation 3.1}$$

In Equation 3.1, R_{final} is the final radius of the hole, and $R_{initial}$ is the initial radius before cold expansion.

In this study, *RE* values were determined by using a digital caliper to measure the hole diameter before and after expansion. The average hole diameter was determined by taking 10 measurements around the hole on each side of the specimen, for a total of 20 hole diameter measurements for each specimen configuration. These 20 measurements were subsequently averaged to obtain a single value of hole diameter for the specimen.

3.3.2.3 Metallurgical Investigation

A metallurgical investigation was performed to analyze grain size around the drilled hole in the steel specimens using an optical microscope. A control specimen, pressure-only treated specimen, and a PICK-treated specimen were each examined at a magnification of 500x.

3.3.2.4 Hardness Measurements

Microhardness readings were taken along several paths on different cut surfaces of the samples sent to the metallurgical laboratory. The microhardness readings were converted from the Vicker's hardness scale to the Rockwell hardness B scale using tables in ASTM E140. The hardness values were further converted from Rockwell hardness B to ultimate tensile strength using a conversion table in Moniz (1994).

3.3.2.5 Neutron Diffraction

Neutron diffraction measurements were performed at the Oak Ridge National Laboratory's (ORNL) Second Generation Neutron Residual Stress Mapping Facility (NRSF2), which is located at the HB-2B beam line at the High Flux Isotope Reactor (HIFR). A University of Kansas PhD student, Gary Simmons, worked with Oak Ridge staff for approximately two weeks on-site at the ONRL to perform the measurements.

3.4 Investigation into Cross-Frame Layout and Skew Effects

An analytical investigation was performed to examine the effects of cross-frame layout and skew angle on distortion-induced fatigue susceptibility of steel bridges. Since distortion-induced fatigue susceptibility and repair effectiveness in skewed bridges has not been a prevalent topic in the literature, the intent of this portion of the study was to improve the body of knowledge in this information arena, improving and broadening the benefits of the research measures developed and studied under TPF-5(189). A brief summary of the methods used in these analyses are described in the following, while more details can be found in Appendix D.

The effects of skew angle, cross-frame spacing, cross-frame layout, cross-frame stiffness, and load placement on the potential for distortion-induced fatigue damage in steel bridges was investigated by performing a suite of more than 1,000 analysis jobs of high-resolution 3D finite element models in Abaqus v.6.8.2 (SIMULIA 2008). Three types of bridge layouts were considered, in which the cross-frames were arranged in a skewed-parallel configuration (Figure 3.21a), skewed-staggered configuration (Figure 3.21b), and skewed-unstaggered configuration (Figure 3.21c). Skew angles of configurations evaluated ranged between 0° and 50°, and cross-frame spacing ranged from 2.3 to 9.1 m (7.5 to 30 ft). Susceptibility to fatigue damage was quantified in terms of computed stress demand in the web gap region of the girders using a HSS-based approach.

(a)Skewed-parallel

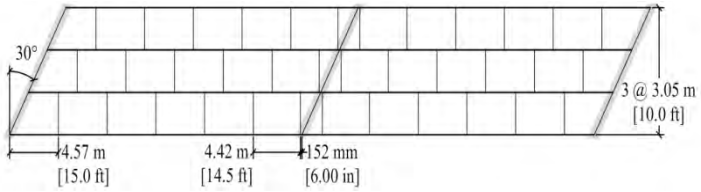

(b) Skewed-staggered

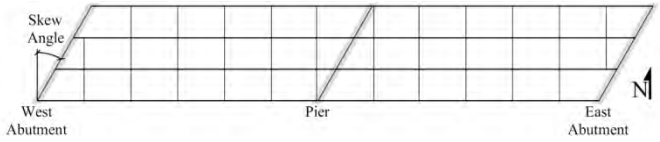

(c) Skewed-unstaggered

Figure 3.21: Bridge layouts (30° skew with 4.6 m (15 ft) cross-frame spacing shown)

The baseline bridge configuration used for the parametric analysis was adapted from American Iron and Steel Institute (AISI) Design Example 2 (1997). The bridge studied was a continuous, two-span bridge with a composite deck and four 978 mm (38.5 inch) deep steel girders spaced at 3 m (10 ft).

Cross-frames used in all bridge layouts studied consisted of three equal-leg angle sections oriented in an X-type configuration. In skewed-parallel configurations, cross-frame length increased with skew angle and bent plate connection plates were modeled taking into account construction considerations, making both cross-frame element and connection stiffness important parameters. A secondary study was conducted to ensure cross-frame element/connection stiffener (angle/stiffener) combinations were selected to have approximately constant stiffness, such that the effects of skew angle, cross-frame layout, cross-frame spacing, and load placement could be evaluated independently from the effect of cross-frame stiffness.

Detailed three-dimensional finite element (FE) models of the entire bridge superstructure were created using Abaqus v.6.8-2 (Simulia 2008). All materials were modeled as linear-elastic. Girders were defined as having a steel material model with a modulus of elasticity of 200,000 MPa (29,000 ksi) and Poisson's ratio of 0.30. The concrete deck was modeled with a modulus of elasticity of 24,850 MPa (3,605 ksi) and Poisson's ratio of 0.15. The mesh was highly refined in the web gap regions, while a maximum mesh size of 51 mm (2.0 inch) was used for other steel parts; all elements were solid type, the majority being eight-node brick elements. A mesh sensitivity analysis was performed before selecting a 152 mm (6.0 inch) mesh size for the concrete deck solid elements, making the bridge deck two elements thick. Surface-to-surface tie constraints were used to attach parts, and welds (modeled with solid elements and attached to the joined surfaces with tie constraints) were used to connect the web to the top and bottom flanges, connection stiffeners to the webs, and cross-frames to connection stiffeners. Interaction between connection stiffeners and girder flanges was defined using hard contact, which caused the connection stiffeners to bear on girder flanges when flange rotation was significant. The models each contained approximately 4 million elements and 27 million degrees of freedom.

Influence and envelope surfaces were constructed to show the relationship between load placement, location of the maximum web gap stress, and the magnitude of the maximum web gap stress. Once optimal load placement was determined through use of the influence surfaces, loads were applied to bridge models in the form of the AASHTO (2013) fatigue truck to induce the maximum principal stress demand in web gaps. A view of one of the finite element models is shown in Figure 3.22.

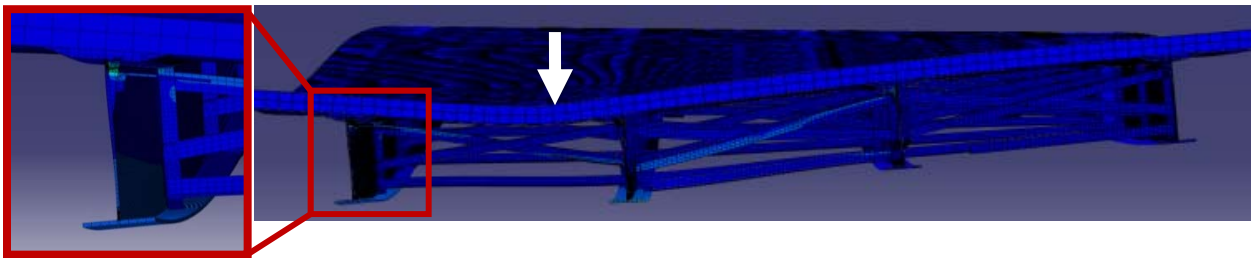

Figure 3.22: Overview of finite element model

Chapter 4: Results and Discussion

4.1 Angles-with-Plate Retrofit

The angles-with-plate retrofit was developed and tested using three different techniques, and the results for each are presented separately:

- A series of physical tests performed on 2.8 m (9.3 ft) long girder models (Section 4.1.1);
- A series of physical tests performed on a three-girder, 9.1 m (30 ft) long steel bridge system (Section 4.1.2), and
- A series of computational simulations (Sections 4.1.3 to 4.1.4) to complement the physical girder and bridge system tests.

4.1.1 Physical Testing Performed on Girder Segments

A total of 14 test trials were performed on three girder subassemblies. Crack progression noted for the various trials is summarized in Table 4.1 and illustrated in Figures 4.1 to 4.3. Specimen 1 was primarily used to calibrate the FE model, and results from testing that specimen are discussed in Appendix A.1.

Five different test trials were conducted using Specimen 2. Of particular interest are Test Trials 2, 3, and 5, which were performed while the angles-with-plate retrofit was applied to the specimen (the other trials were performed in the unretrofitted condition to grow the cracks to longer lengths). As shown in Figure 4.1, no crack growth was observed in the bottom web gap of the specimen, and minimal crack growth was observed in the top web gap while the retrofit was installed in those respective regions.

Eight test trials were performed on Specimen 3. Trials 2, 4, 6, and 8 were performed in the retrofitted condition. As can be observed in Figures 4.2 and 4.3, no crack growth was experienced in either the bottom or top web gaps while the retrofit was in place.

Table 4.1 Crack Progression

Specimen/ Trial	Retrofit Measure/Observation	Number of Cycles - Trial	Number of Cycles - Specimen	Crack Location and growth, mm (inch)			
				Bottom Horiz.	*Bottom Horseshoe*	*Top Horiz.*	*Top Horseshoe*
1/1	*No Retrofit / Crack initiation*	250,000	250,000	0 (0)	6 (0.3)	0 (0)	0 (0)
1/1	*No Retrofit / Crack growth*	740,000	990,000	6 (0.3)	25 (1)	0 (0)	0 (0)
2/1	*No Retrofit / Crack initiation*	24,460	24,460	0 (0)	6 (0.3)	0 (0)	0 (0)
2/1	*No Retrofit / Crack growth*	490,460	514,920	203 (8)	127 (5)	0 (0)	0 (0)
2/2	*Angles Bottom*	1,225,860	1,740,780	0 (0)	0 (0)	57 (2.3)	25 (1)
2/3	*Angles Bottom & Top*	1,250,740	2,991,520	0 (0)	0 (0)	25 (1)	0 (0)
2/4	*Crack Stop Holes*	39,720	3,031,240	13 (0.5)	70 (2.8)	0 (0)	0 (0)
2/5	*Angles Bottom & Top*	1,238,300	4,269,540	0 (0)	0 (0)	0 (0)	0 (0)
3/1	*No Retrofit / Crack initiation*	73,000	73,000	0 (0)	10 (0.38)	0 (0)	0 (0)
3/1	*No Retrofit / Crack growth*	276,000	349,000	51 (2)	41 (1.6)	0 (0)	0 (0)
3/2	*Angles Bottom*	1,200,000	1,549,000	0 (0)	0 (0)	0 (0)	0 (0)
3/3	*No Retrofit / Crack growth*	71,700	1,620,700	51 (2)	0 (0)	0 (0)	0 (0)
3/4	*Angles Bottom*	1,200,000	2,820,700	0 (0)	0 (0)	0 (0)	0 (0)
3/5	*No Retrofit / Crack growth*	322,000	3,142,700	51 (2)	19 (0.75)	0 (0)	10 (0.38)
3/6	*Angles Bottom*	1,200,000	4,342,700	0 (0)	0 (0)	0 (0)	0 (0)
3/7	*No Retrofit / Crack growth*	275,000	4,617,700	54 (2.1)	13 (0.5)	0 (0)	0 (0)
3/8	*Angles Bottom*	1,200,000	5,817,700	0 (0)	0 (0)	0 (0)	0 (0)

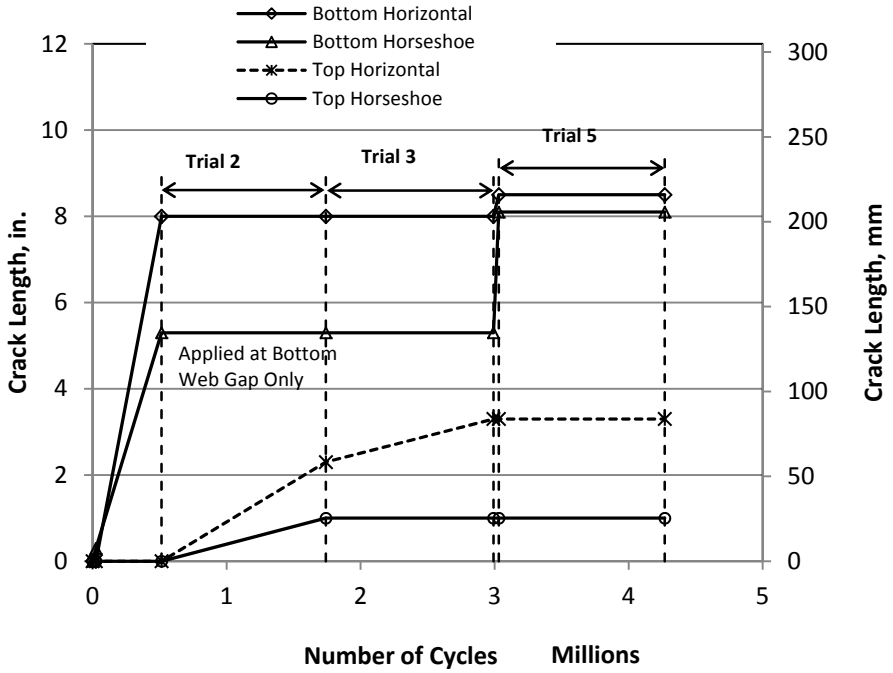

Figure 4.1: Crack growth for Specimen 2

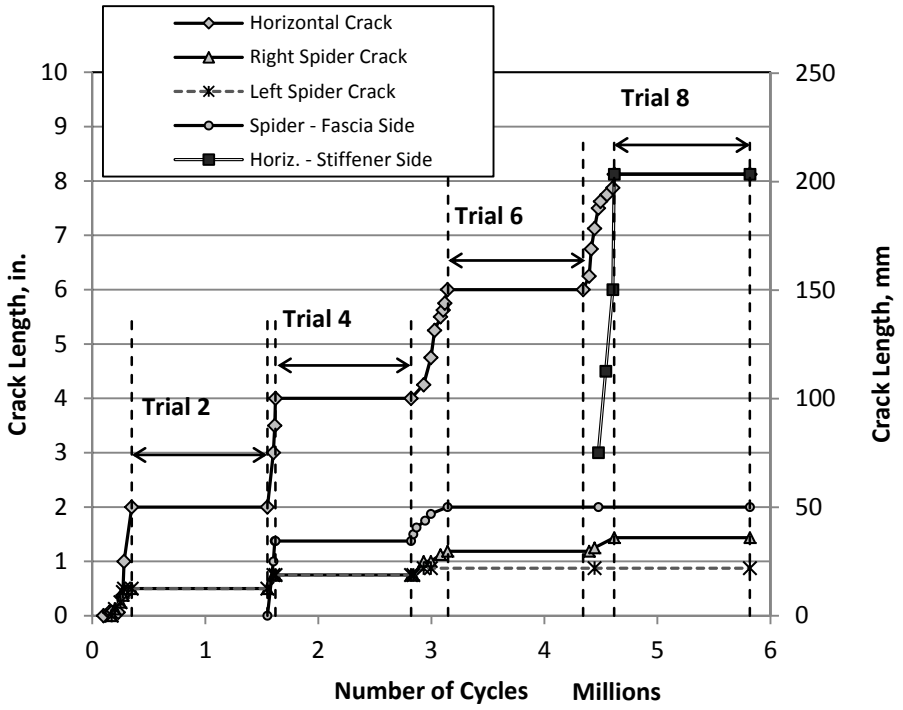

Figure 4.2: Horizontal (web-to-flange weld) crack growth for Specimen 3

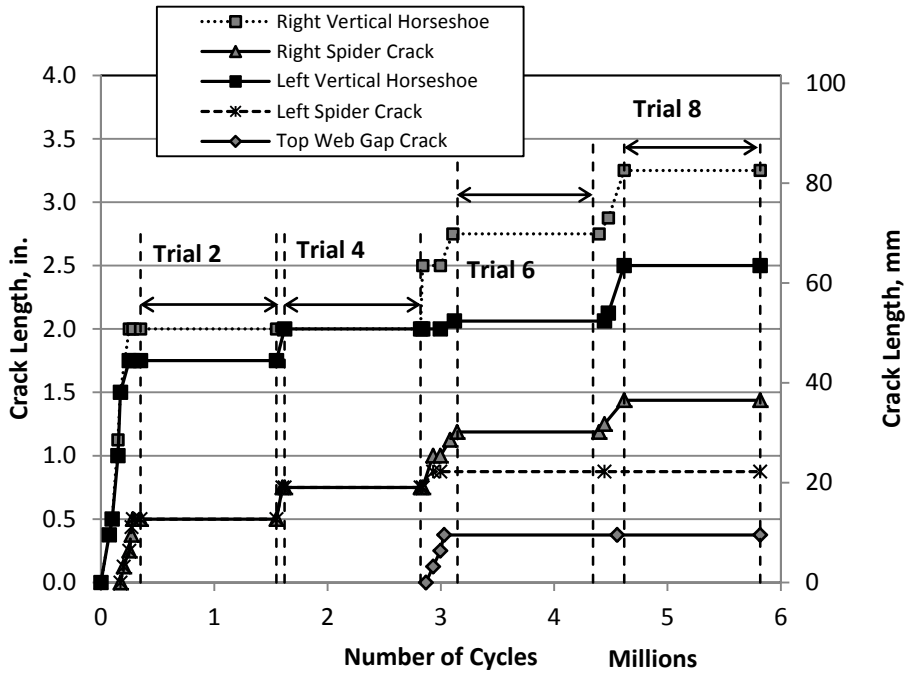

Figure 4.3: Horseshoe-shaped (connection plate-to-weld) crack growth for Specimen 3

The trials conducted with Specimen 3 showed that, for the applied stress range and all crack geometries evaluated, the angles-with-plate retrofit measure prevented crack growth in the web gap region that was repaired. This is an important consideration because it simplifies the implementation of this retrofit measure by allowing the use of a single-size configuration for various web gap regions of the same bridge, regardless of crack length.

The results of this test sequence showed that the angles-with-plate retrofit exhibited significant merit in repairing distortion-induced fatigue cracking. Therefore, the angles-with-plate retrofit was subsequently evaluated in the more realistic model, the three-girder bridge.

4.1.2 Physical Testing Performed on Test Bridge

Results of testing the angles-with-plate retrofit on the test bridge are summarized in Figures 4.4 and 4.5, which presents the results of 14 separate fatigue test trials. The results have been separated between the two exterior girders, labeled as the “North” (N) girder (Figure 4.4) and the “South” (S) girder (Figure 4.5)

Figures 4.4 and 4.5 present crack propagation levels between test trials surrounding the connection plate-to-web weld, which is the location that first presented cracking in this series of tests. In these plots, the dashed lines each represent the end of test trial. Test Trial 1N and Trial 1S are the only trials in the test series that did not include a retrofit configuration; these trials were performed to initiate and propagate cracking in the web gap region.

As shown in Table 3.2, the force range applied to the test system was increased successively and significantly throughout the sequence, representing a highly demanding test of the angles-with-plate retrofit. Test Trials 1 and 2 were performed at a load range of 240 kN (54 kips); Test Trial 3 was performed at a load range of 320 kN (72 kips); Test Trials 4 and 5 were performed at a load range of 400 kN (90 kips); and Test Trials 6 and 7 were performed at a load range of 480 kN (108 kips). The crack propagation data presented in Figures 4.4 and 4.5 has not been normalized in any way to account for these increasing loads; instead measured crack growth throughout the entirety of the test has been presented. In other words, the performance noted in later trials was achieved under higher load demands than under the earlier trials.

The data for crack propagation surrounding the connection plate-to-web weld in the North and South girders shows strong performance of the angles-with-plate retrofit at drastically slowing crack propagation under demanding levels of distortion-induced fatigue.

During Test Trials 4 and 7, fatigue failures of a cross-frame element were experienced (shown in Figure 4.6). In both cases, the cross-frame at the center of the bridge, between the North and Center girders, experienced fatigue failure – in its tab plate in Trial 4N and through the horizontal member in Trial 7N. After the cross-frame failure in Trial 4N, the cross-frame was repaired by welding and replaced in the model so that testing could continue. Since the cross-frame failure in Trial 7N occurred at the end of the test sequence, it was not repaired. These failures were significant test events for three reasons:

1. Load redistribution is expected to have occurred within Test Trials 4 and 7, therefore, the results for those trials have been shaded in Figure and Figure;
2. The demand placed upon the bridge was large enough in both cases to produce failures in the cross-frame tabs – a fatigue failure that is not commonly observed in the field, while distortion-induced fatigue cracking is fairly commonplace; and
3. The cross-frame tab failures implied that the angles-with-plate retrofits had shifted the most susceptible detail from the web gaps to the cross-frame tabs.

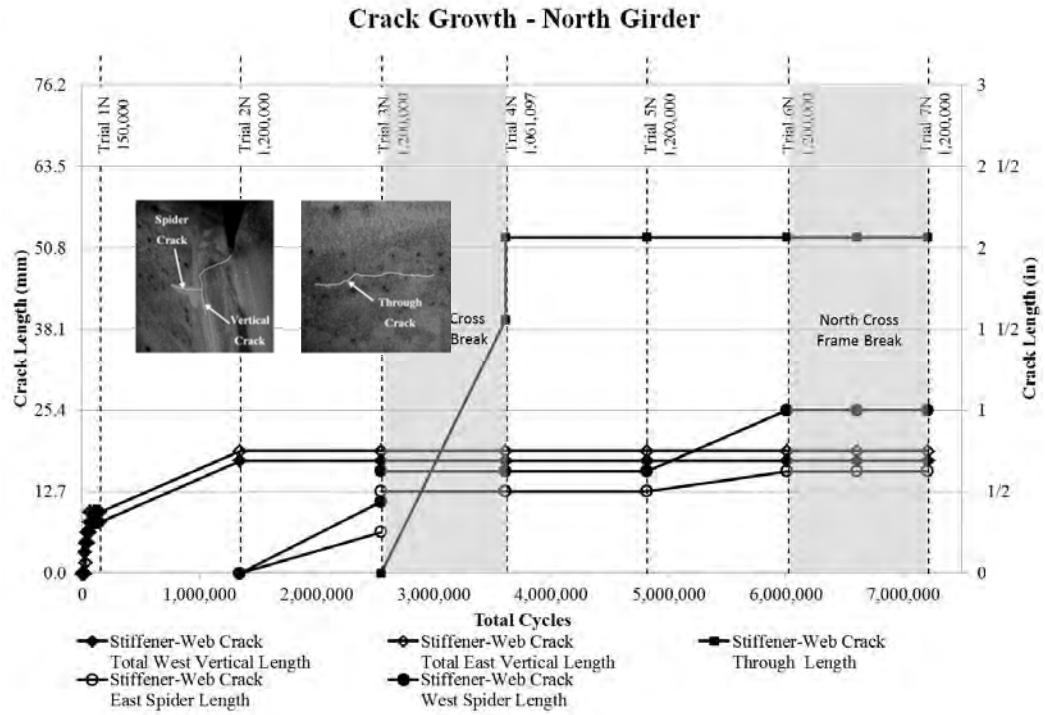

Figure 4.4: Crack growth – North girder

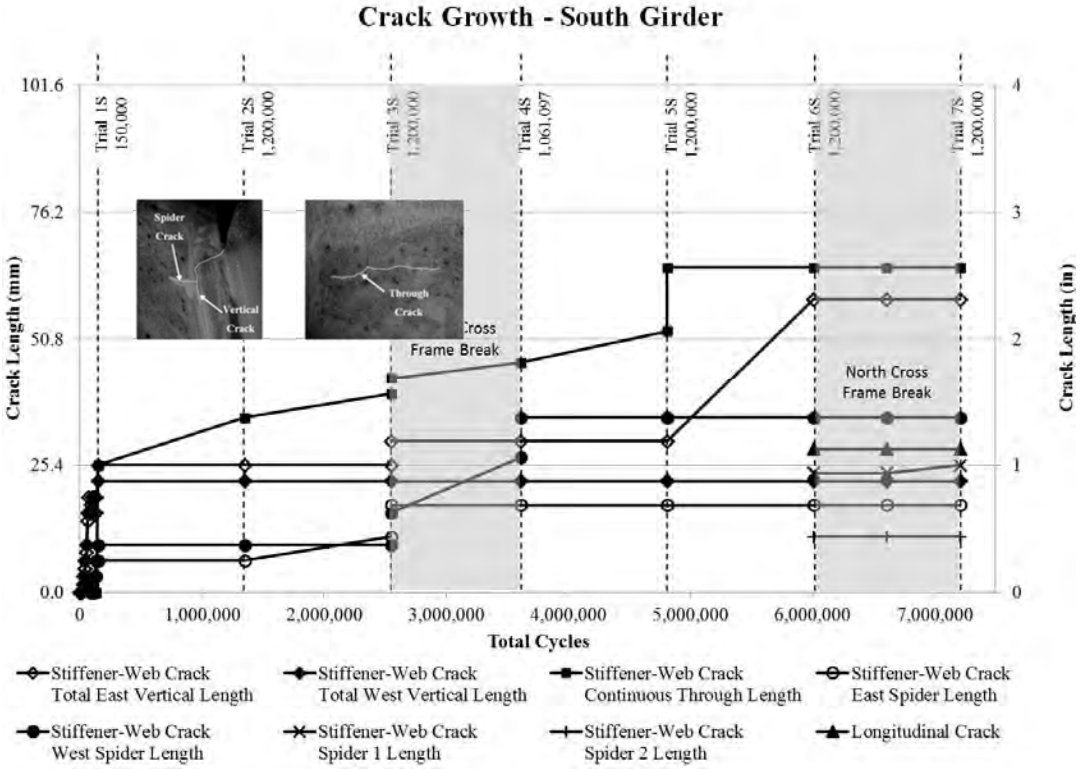

Figure 4.5: Crack growth – South girder

Figure 4.6: North cross frame failure during Trial 4N

A horizontal crack formed between the web and the top flange in the North girder, and was identified at the end of Trial 6N. The crack was 298 mm (11¾ inch) long at the time of discovery; due to very small crack opening displacements, the crack was extremely difficult to detect, even under dye penetrant and UV light. The web-to-flange regions had been inspected through the test sequence, but it was not possible to determine whether the crack went undetected over multiple trials, or if it developed during Trial 6N. It is hypothesized that the initiation of the web-to-flange crack was due in some part to the failure of the cross-frame in Trial 4N, and the extremely high load levels used in this portion of the test sequence are again emphasized here. Crack-arrest holes were installed after Trial 6N to allow for further testing of the south girder, but the crack re-initiated at the weldment during Trial 7N and propagated in unstable crack growth. The crack was then re-welded to allow for continued testing of Trial 7S. However, at this point the re-welded crack at the web-to-flange weld extended nearly beyond the footprint of the angles-with-plate retrofit, and reinitiated. Based on these findings, the authors do not recommend the angles-with-plate retrofit for long web-to-flange weld cracks.

It is also noteworthy that after repeated detailed, methodical crack inspection on the South girder, a web-to-flange weld crack was never detected during the course of the testing.

A more comprehensive discussion of all of these results are provided in Appendix A.3

4.1.3 Computational Simulations of Girder Segments

Parametric analyses of the angles-with-plate retrofit measure were performed to determine the optimal back plate and angle dimensions. The first parametric study involved varying the thickness of the angles and back plate within the finite element model, while other dimensions were kept constant. In general, the parametric study showed that increasing the stiffness of the retrofit elements reduced stress demands at both the connection plate-to-web weld and the web-to-flange weld. It is important to emphasize that although the stiffness of the angles and the plate did have a significant effect on the calculated stress demand, in all instances the calculated stress demands at both the CP-to-web weld (HSS 1) and the flange-to-web weld (HSS 2) were much lower than the values computed for the unretrofitted configuration. Nonetheless, these results strongly indicate that retrofit dimensions (and thus, stiffness) could be chosen to optimize performance for specific crack types.

From a broader perspective, the magnitude of reduction in stress demand clearly shows that, for the range of thicknesses studied, the angles-with-plate retrofit measure significantly reduced the computed stress demand at the critical locations of the bottom web gap region [Figure 4.7(a) vs. Figure 4.7(c)], regardless of connecting element thickness. Stress contours in Figure 4.7(c) were chosen so that the colors would correspond to the same stress ranges in both figures. It is clear from the comparison that the reduction in stress demand was very significant and that it occurred throughout the entire web gap region, and not only at the critical points.

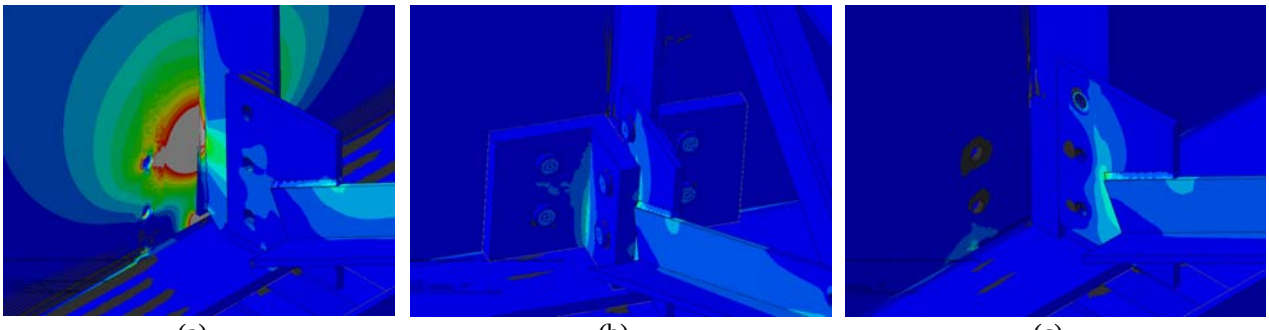

(a) (b) (c)

Figure 4.7: (a) Computed maximum principal stresses without retrofit, (b) Angle retrofit configuration, (c) Computed stresses with retrofit
Scale is set so that red values are equivalent to 345 MPa (50 ksi) in all figures.

A second parametric study was performed in which the angle and back plate thickness were kept constant at 13 mm ($^1/_2$ inch), while the length of the back plate was changed. Extremely low levels of variation were found to occur in HSS1 and HSS2 across this parametric study. The results suggest that it is counterproductive to increase the length of the back plate, and that a configuration with a back plate with a length of 1.5 times the length of the horizontal web-to-flange crack provided excellent results while remaining manageable during field installation.

The findings from the computational simulations of the angles-with-plate performance evaluated in the girder segment set-up are discussed in detail in Appendix A.2 of this report.

4.1.4 Computational Simulations of the Test Bridge

Results from the computational simulations for the angles-with-plate retrofit applied in the test bridge have been presented in Appendix A.4. In addition to examining: (1) the changing stress demand in the web gap region with varying crack length, (2) the effect of deck cracking (studied by reducing gross deck stiffness), and (3) the effect of a broken cross-frame, a parametric analysis was also performed in which the relative performance of various retrofit measures were compared, including three variations of the angles-with-plate retrofit technique. The retrofit measure performance was evaluated when applied over uncracked geometry and geometries with varied crack lengths.

The results shown in Figure 4.8 are representative of the results for four retrofit measures compared against the case in which no retrofit was applied. Results shown are for a single crack length, and more detailed discussions regarding the effect of crack length are provided in Appendix A.4. The four retrofit measures compared here are:

- The angles-with-plate retrofit (13 mm ($^1/_2$ in.) thickness)
- The angles-with-plate retrofit (19 mm ($^3/_4$ in.) thickness)
- The stiffened angles-with-plate retrofit (19 mm ($^3/_4$ in.) thickness)
- The conventional retrofit connecting the connection plate to the top flange with bolted angles (19 mm ($^3/_4$ in.) thickness).

From the model including cracked geometry but no retrofit, it can be observed that an initial horseshoe-shaped crack length of 51 mm (2 in.) resulted in a connection plate-web weld hot spot stress of approximately 72% of the uncracked state, while the flange-web weld hot spot

stress was approximately 41% of the uncracked state. Retrofit performance was based on additional reduction from the cracked state.

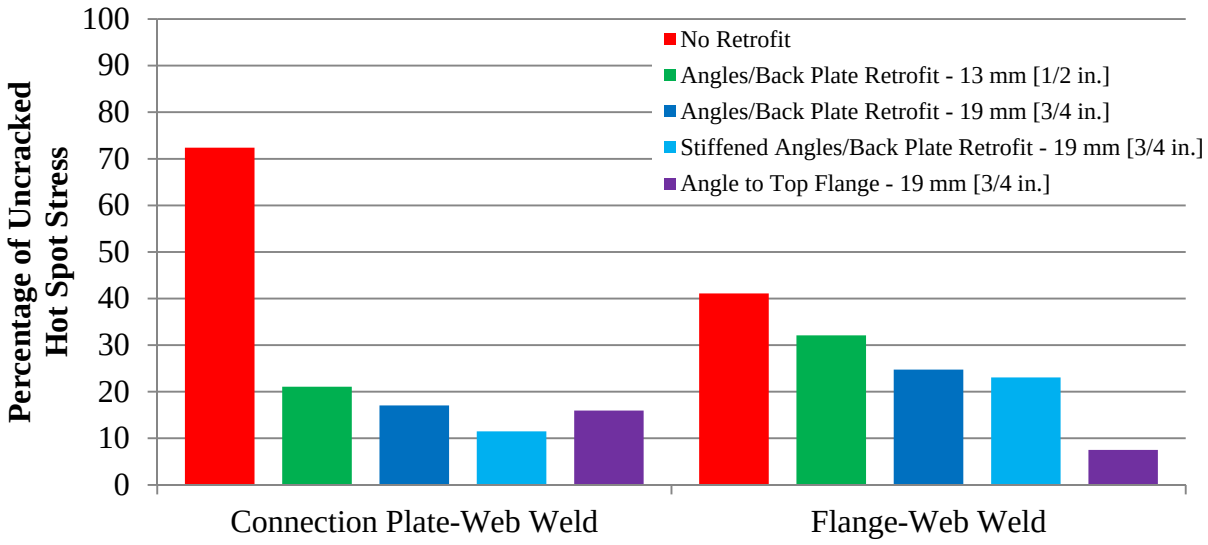

Figure 4.8: Percentage of uncracked hot spot stresses for connection plate-web weld and flange-web weld with various retrofit conditions and a 51 mm (2 inch) horseshoe crack

Based on all models studied, the best retrofit measure for reduction of hot spot stress around the connection plate-web weld was found to be the stiffened angles-with-backing plate (as shown in Figure 3.10b). This finding was corroborated by the simulations of the girder models, which also indicated that stiffer retrofits were more effective than more flexible retrofits.

For reducing crack growth propensity at the flange-to-web weld, it was found that the best performing retrofit measure was the angles connected to the girder top flange. Although this traditional retrofit indicated good performance, these findings must be balanced considering the required additional welding and/or deck removal with traffic disruption for field implementation. It should be noted that the stiffened angles-with-plate retrofit did provide a stress decrease at the web-to-flange weld on the order of 50%, and it is anticipated that this level of stress reduction will be adequate to halt crack initiation/propagation for many field applications.

In summary, results from the analytical comparison of the various retrofits indicated that the stiffened angles-with-plate retrofit is extremely effective for repairing cracking around the

connection-plate-to-web-weld. The results also indicated that the stiffened-angles-with-plate retrofit is effective for reducing stress demands at the web-to-flange weld. However, if the web-to-flange weld is showing high propensity for crack growth, the results indicate that a traditional angle-to-top flange retrofit may be a more effective choice for repair.

4.2 Fiber-Reinforced Polymer Retrofit Measures

Results from the series of tests and analyses aimed at studying applications of Fiber-Reinforced Polymer (FRP) retrofit measures are presented in this section. The results have been organized as follows:

- Testing of small-scale bending-type and tension-type fatigue specimens. (Sections 4.2.1 and 4.2.2);
- Physical tests performed within the girder segment test set-up in which two primary techniques were developed and tested (Section 4.2.3):
  - A composite block retrofit
  - A variation of the angles-with-plate retrofit that included a layer of carbon fiber reinforced polymer (CFRP) material sandwiched between the steel girder and the steel retrofit elements
- Computational simulations complementing the above physical investigations. (Section 4.2.4).

4.2.1 Physical Testing Performed on Tensile Fatigue Specimens

Results of physical tests performed on tensile fatigue specimens repaired with CFRP overlays showed that as stress range was increased, a greater stiffness ratio was required for the fatigue crack propagation life to tend towards infinity. At 166 MPa (24 ksi), 221 MPa (32 ksi), and 263 MPa (38 ksi) the number of cycles to failure tended towards infinity at stiffness ratios of 0.8, 1.0, and 1.6, respectively. The experimental results showed a diminishing effect on stress demand as the stiffness ratio increased. Based on these results it is the opinion of the authors that the greatest benefit of using overlays to reduce the stress demand is achieved for stiffness ratios below unity.

The results showed that bonding of pre-fabricated multi-layered CFRP overlays increased the theoretical fatigue crack propagation life of unretrofitted steel specimens by at least three times and up to 162 times before experimental specimens reached run-out.

The observed increase in fatigue-crack propagation life matched or was significantly higher than values ranging between 3 and 10 reported in previous studies on aluminum plates, steel plates, and steel beams. The main difference between the overlays used in this study and those used in other studies is that the stiffness ratio *SR* was significantly higher in this study than identified in previous literature.

Data from this test sequence have been presented in Appendix B.1, along with detailed analysis of the results.

4.2.2 Physical Testing Performed on Bending Fatigue Specimens

Physical tests of CFRP overlays applied to bending fatigue specimens showed that using CFRP overlays was highly effective both as a preventive measure to extend the fatigue-crack initiation life of welded connections and as a repair measure to reduce the stress demand in welded connections below the crack propagation threshold. An improvement in fatigue-crack initiation life of at least 9.0 times was recorded for specimen TRI 06, and at least 9.5 times for specimen TRI 07, when compared with the fatigue-crack initiation life of untreated steel specimens tested at the same stress range. Composite overlays were found to be as effective as other established repair methods such as ultrasonic impact treatment (UIT), which have been shown to provide significant improvements in fatigue-crack initiation life (14x, reported by Vilhauer [2010]).

Detailed data from this test sequence have been presented in Appendix B.2 and B.3, along with detailed analysis of the results.

4.2.3 Physical Testing Performed on Girder Models

4.2.3.1 Composite block retrofit

Results of the physical test of a girder model loaded in distortion-induced fatigue and repaired with a composite FRP block showed that the fatigue life of the specimen was improved significantly. Figure 4.9(a) presents the crack pattern that was recorded during the inspection directly before applying the composite block retrofit (after Trial 1 was completed and before Trial 2 was completed), and Figure 4.9(b) presents the crack pattern recorded after Trial 2 was completed with the retrofit (after 1.2 M cycles). It can be observed that the only crack that

initiated after application of the retrofit was a small spider crack on the right side of the connection plate. The retrofit applied in this study was only applied on the interior face of the girder.

Further discussion of the findings from this test sequence can be found in Appendix B.4.

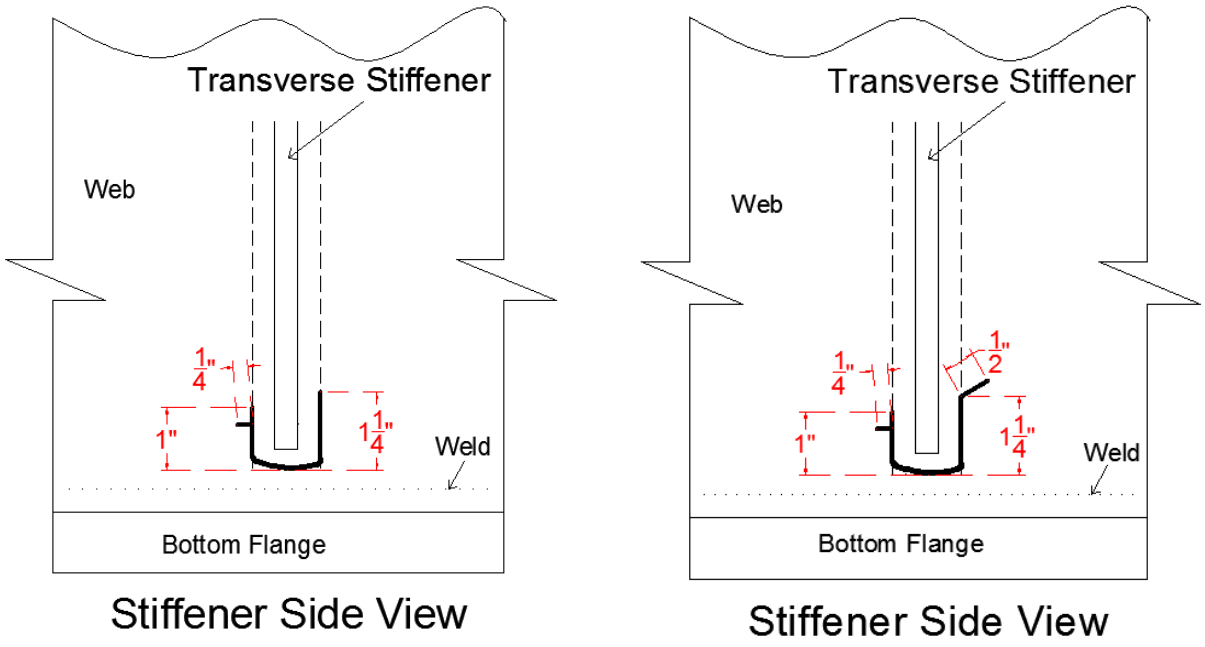

Figure 4.9: Recorded crack patterns
(a) after Trial 1 (without FRP block retrofit); (b) After Trial 2 (with FRP block retrofit)

4.2.3.2 Angles-with-plate retrofit with CFRP

Inspection of the girder segment specimen after Trial 1 (steel-only angles-with-plate retrofit) and Trial 2 (angles-with-plate with CFRP sandwiched layer) indicated that cracks did not propagate during either test trial. The original (repaired) crack length was equal to approximately 50% of the depth of the web, and extended vertically along the connection plate-to-web weld. Therefore, the physical test results, in terms of crack propagation, showed that the retrofit applied worked very satisfactorily in both configurations (with and without CFRP) for a very severe web crack loaded in out-of-plane fatigue. The analytical component to this portion of the study (described in 4.2.4.3.2) is useful for further distinguishing between the two measures.

Further discussion of the findings from this test sequence can be found in Appendix B.6.

4.2.4 Computational Simulations of FRP Retrofit Measures

4.2.4.1 Computational Simulations of Tensile Fatigue Specimens

Computational simulations performed to investigate the tensile fatigue specimens with bonded CFRP overlays yielded the following summary results.

The relationship between the modulus of elasticity of the CFRP, E_{CFRP}, and stress imposed on the steel specimen was found to be parabolic in nature and inversely proportional, indicating that there was a significant advantage associated with using an overlay, even if E_{CFRP} was relatively low. Similar to the finding for the modulus of the CFRP overlay, it was found that increasing the thickness of the CFRP exhibited diminishing returns. It was determined that the magnitude of stress reduction in the steel specimen was not significantly affected by whether the CFRP stiffness was changed through increasing the modulus or through increasing the overlay thickness.

The effect of the bond layer thickness (between the steel and the CFRP) was also investigated through the simulations, and it was found that the thickness of the interface layer may not be relevant to fatigue-crack propagation life due to the negligible effect on the stress range, but it is a very important parameter in terms of the bond performance of the interface layer under cyclic loading.

4.2.4.2 Computational Simulations of Bending Fatigue Specimens

It was found that using CFRP overlays was highly effective both as a preventive measure to extend the fatigue-crack initiation life of welded connections and as a repair measure to reduce the stress demand in welded connections below the crack propagation threshold.

The simulations showed that the geometric profile of the CFRP overlay did not have a significant effect on the calculated stress demand at the weld toe, whereas the presence of a gap between the weld and the CFRP overlay did have a notable detrimental effect. Of the remaining parameters, it was found that the modulus of elasticity of the composite and the thickness of the interface bond layer had the most significant effect on the stress demand at the weld toe.

Further details regarding the results from computational simulations for the bending fatigue specimens can be found in Appendix B.2 and B.3.

4.2.4.3 Computational Simulations of Girder Model

4.2.4.3.1 Composite block retrofit measure

Results from the finite element models of the girder model with the composite block installed showed very significant stress demand decreases surrounding the connection plate-to-web-weld and the web-to-flange weld. Both decreases were greater than 90% of the stress demands in the unretrofitted state. However, it is emphasized here and in Appendix B.4 that since some physical debonding was noted during physical testing these results should be viewed as an upper bound of behavior, to be expected only if perfect bond is maintained between the steel and the CFRP block. It is noted that the physical test results, rather than the FE results for this particular retrofit, are expected to be more indicative of the behavior of this retrofit.

4.2.4.3.2 Sheet-Type CFRP + Steel Repair

To determine the effectiveness of the version of the angles-with-plate repair tested for deep web gaps, a series of finite element models were studied (described in greater detail in Appendix B.5) The FE models were not identical to the physical models, however, they were similar enough in nature to be considered contextually useful. Girder models were simulated with two different crack lengths: $1/8^{th}$ the depth of the web and ¼ the depth of the web.

Based on the results from all the FE models with crack-stop holes (Figure 4.10 and 4.11) it was found that while drilling crack-stop holes is effective in reducing the peak demand at the tip of the crack by removing damaged material from the fracture process zone, this type of repair is not effective in mitigating stress demands induced by out-of-plane forces in web gap regions, and should be used in combination with other retrofit measures intended to reduce large stress demands induced by geometric discontinuities in the web gap region. Because the primary benefits of drilling crack-stop holes are the removal of the sharp crack tip and fracture process zone, the drilling of large-diameter crack-stop holes is generally not justified, and was shown to be detrimental in some instances.

Repairing the girder web with full depth steel splice plates did provide an alternate load path and generally reduced stress demands (Figure 4.10 and 4.12). Effectiveness of this repair method also increased as the length of the crack increased from $^1/_8$ of the depth of the web to $^1/_4$ of the depth of the web. However, this steel-only repair type did not produce as great of stress reductions as found when the CFRP sheets were used in conjunction with the steel plates.

The use of adhesively bonded CFRP overlays in combination with a 19 mm ($^3/_4$ in.) crack-stop hole and bolted steel cover plates showed drastic reductions in stress in the cracked region of the web when compared with simulation results from un-retrofitted models, models repaired with crack-stop holes, and models repaired with full-depth splice plates (Figure 4.10 and 4.13). The use of a resin layer between the steel web and the CFRP layer was shown to be effective in transferring the high stress demands in the web gap to the CFRP and the steel plate. Bonding the CFRP layer had the effect of distributing the stress over the entire area covered by the repair, eliminating the presence of small regions with highly concentrated stress demands. This smoothing effect is the main benefit of this retrofit measure with respect to the others discussed.

These results are described with additional details in Appendix B.5.

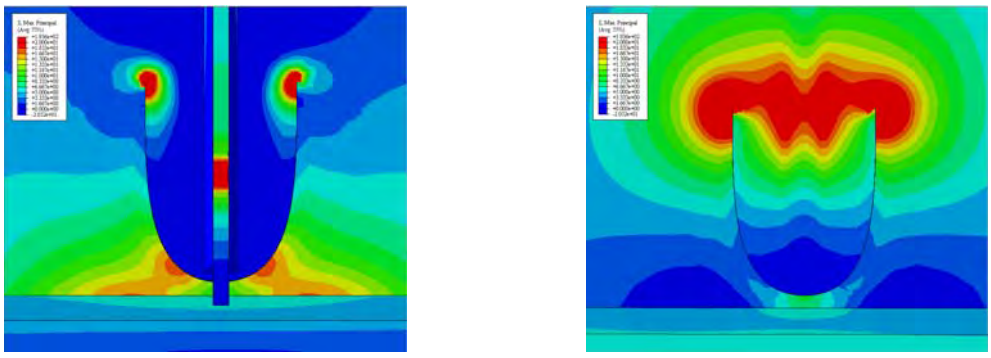

(a) No retrofit – interior **(b) No retrofit – fascia**

Figure 4.10: Maximum principal tension stresses in unrepaired models

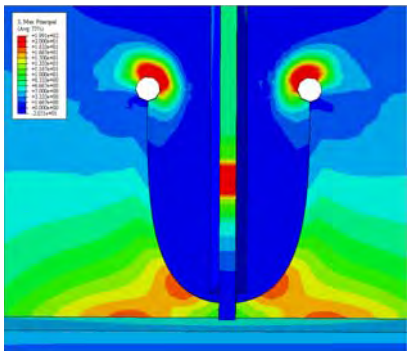

(a) 19 mm (0.75 in.) CSH– interior

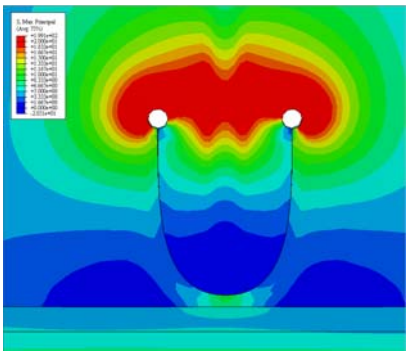

(b) 19 mm (0.75 in.) CSH– fascia

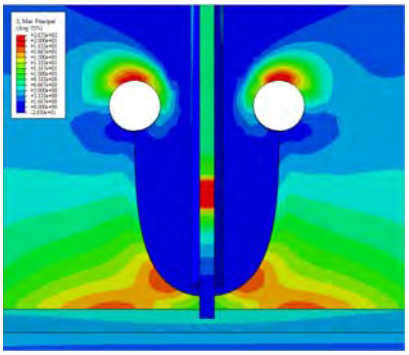

(c) 51 mm (2.0 in.) CSH – interior

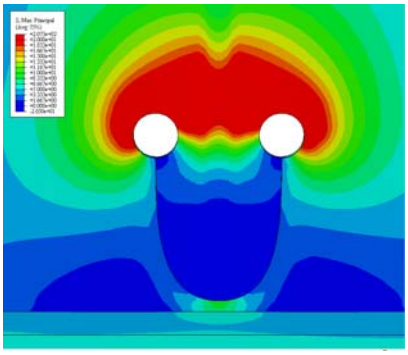

(d) 51 mm (2.0 in.) CSH – fascia

Figure 4.11: Maximum principal tension stresses in models repaired with crack-stop holes under combined loading conditions

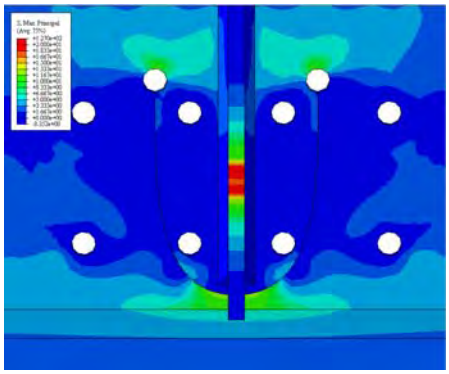

(a) Full-depth splice plate –interior

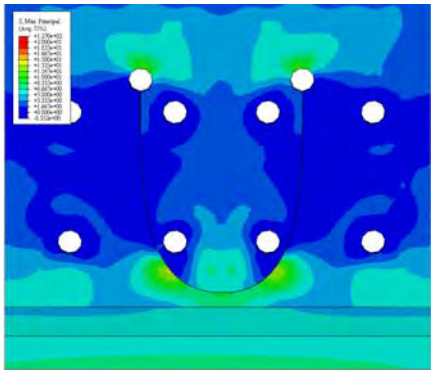

(b) Full-depth splice plate –fascia

Figure 4.12: Maximum principal tension stresses in models repaired with full-depth splice plate

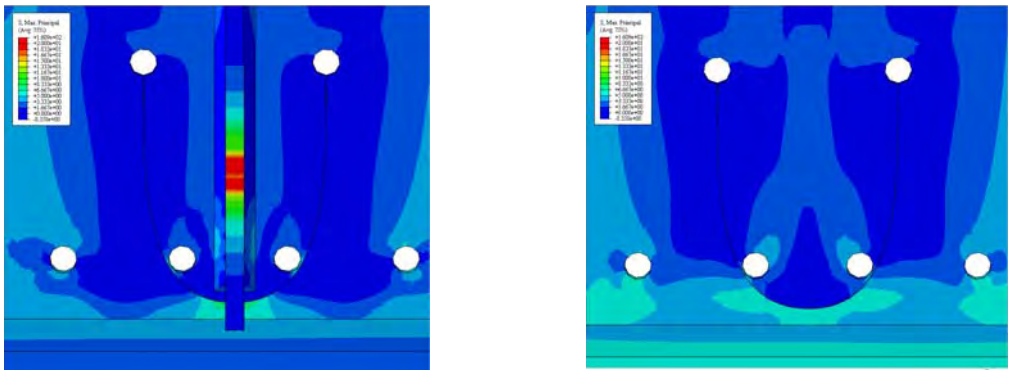

(a) CFRP retrofit system – interior (b) CFRP retrofit system – fascia

Figure 4.13: Maximum principal tension stresses in model repaired with CFRP

4.3 PICK Technology

Results from a series of tests and analyses aimed at developing and investigating the effectiveness of PICK technology for improving the fatigue performance of drilled crack arrest holes are presented in this section.

4.3.1 Analytical Validation of Approach

The 2-D finite element models for an aluminum specimen subjected to cold-expansion produced results for levels of tangential residual stress that were closely comparable in shape and magnitude to previously published finite element model results performed in aluminum. Additionally, it was found that the 2D and 3D steel models exhibited similar levels of tangential residual stresses as found for the aluminum models (Figure 4.14), indicating that a level of 4% cold-expansion could be considered as effective in steel as in aluminum.

Further results from this portion of the study are presented in Appendix C.1.

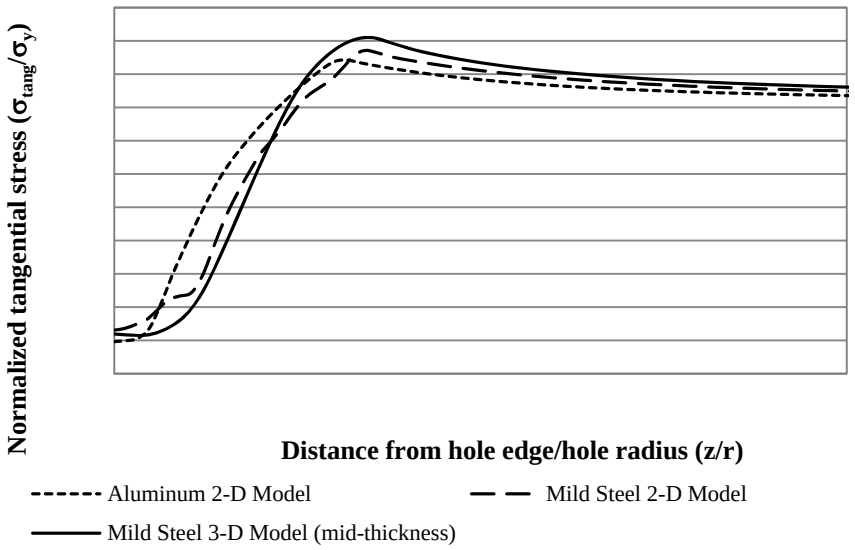

Figure 4.14: Tangential residual stress normalized with respect to material yield strength comparing model results for aluminum and mild steel at 4% uniform expansion

4.3.2 Development of PICK Technology and Testing

4.3.2.1 Fatigue Testing

Experimental results from fatigue testing five control specimens, four pressure-only treated specimens, and six PICK-treated specimens have been presented in Figure 4.15. The figure shows that the three groups of data formed separate data clusters, with the best fatigue performance being exhibited by the PICK-treated specimens, while the pressure-only treated specimens still out-performed the control specimens. The plot also includes the 95% confidence level for the three groups.

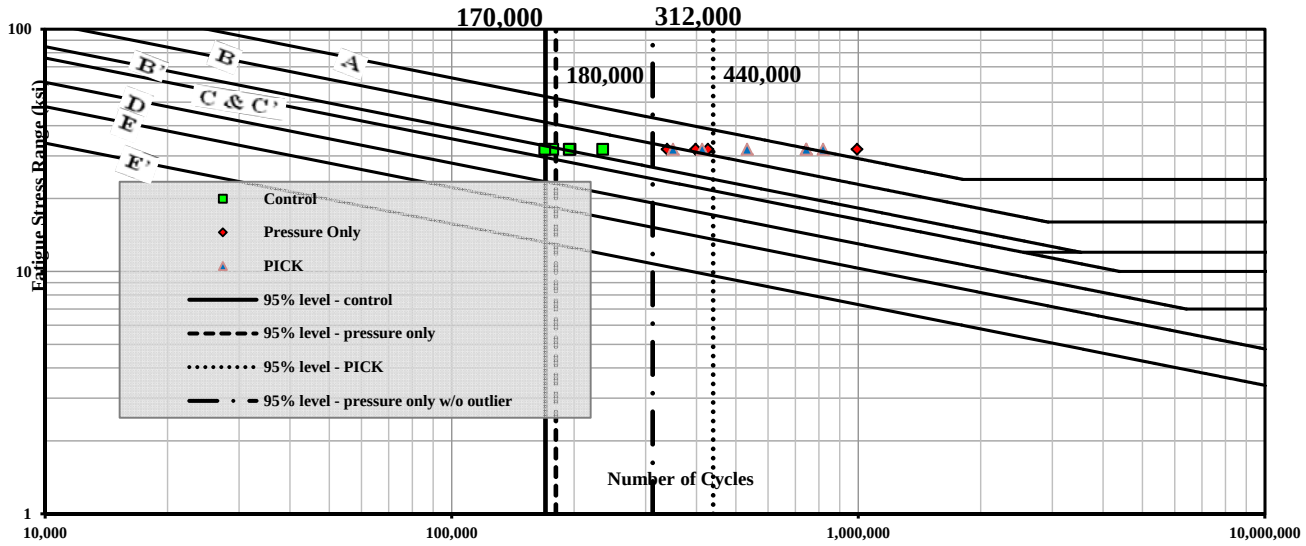

Figure 4.15: Fatigue test results plotted on S-N diagram

4.3.2.2 Retained Expansion Measurements

The hole diameter at the center of each test specimen was measured before and after treatment, for the purpose of calculating retained expansion (*RE*) in each specimen. Levels of measured retained expansion for the pressure-only and PICK-treated fatigue and plate specimens are reported in Appendix C.2.

The measurements for retained expansion showed that PICK-treated specimens achieved higher levels of retained expansion than pressure-only treated specimens. However, the average levels of retained expansion measured for both pressure-only treated and PICK-treated specimens were significantly higher than noted in the literature as being sufficient to extend the fatigue life of a drilled hole. This finding indicates excellent performance of the pressure-only and PICK treatments for imparting meaningful levels of residual compressive stress.

4.3.2.3 Metallurgical Testing

The metallurgical examination that was performed on control, pressure-only, and PICK-treated specimens showed differences in the grain sizes between the three groups. It was observed that pressure-only treated specimens exhibited grain deformations to a depth of approximately 0.008 to 0.009 mm (0.0003 to 0.0035 in.) and PICK-treated specimens exhibited grain deformations to a depth of 0.001 mm (0.0040 in.) from the surface of the hole. This finding lends greater weight to the fatigue test results, which showed measureable differences between the fatigue lives of these three groups. Additionally, the increased level of grain deformations noted between the pressure-only treated and PICK-treated specimens supports the observed increase in retained expansion from the pressure-only specimens to the PICK-treated specimens. Greater discussion regarding the metallurgical testing and microstructure photographs are presented in Appendix C.2.

4.3.2.4 Hardness Testing

Pressure-only and PICK-treated specimens showed an increase in hardness (and by correlation, ultimate strength) over control specimens. For both pressure-only and PICK-treated specimens, hardness decreased approximately linearly with increasing distance from the hole edge.

4.3.2.5 Neutron Diffraction

The tangential, radial, and normal strains measured by neutron diffraction are plotted in Figure 4.16. For the tangential residual strain, the minimum strain was found to be $-1553\mu\varepsilon$, the maximum was $396\mu\varepsilon$, while the elastic-plastic boundary was approximately $r/r_i = 5.6$. Note that the tangential strain near the hole edge ($r/r_i = 1$) appears to show yielding in compression.

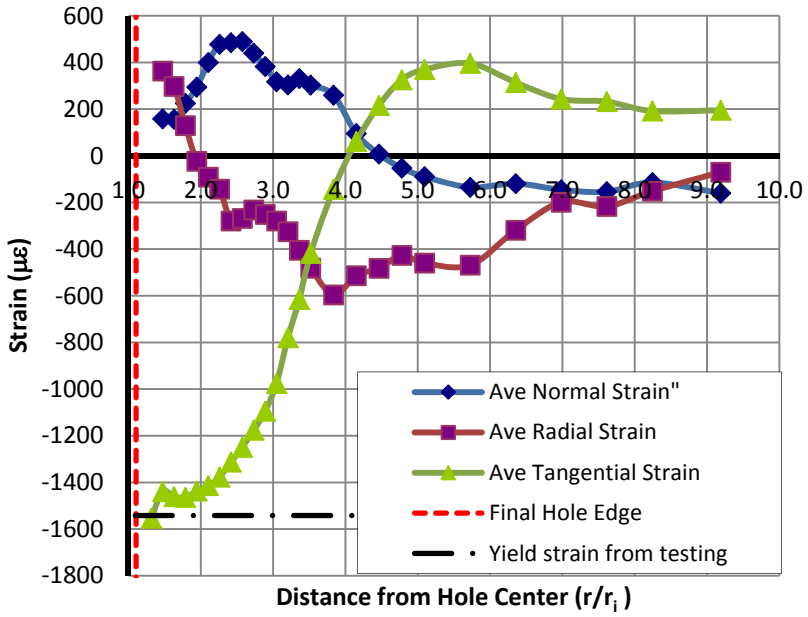

Figure 4.16: Strains in PICK-treated specimen from neutron diffraction measurements taken at ORNL

The shapes of the radial and tangential residual strain, in general, matched the curves of stress calculated from the classic closed-form procedures presented in Nadai (1943) and Ball (1995).

4.4 Cross-Frame Layout and Skew Effects

Two separate paths were used to evaluate the potential for fatigue damage within the finite element models. Maximum principal tensile stress magnitudes were extracted along each path, from both sides of the web, even when cross-frames were not placed back-to-back. The maximum principal tensile stress along each path was adopted as the controlling HSS for that stress path. HSS#1 and HSS#2 are used herein to designate the maximum stress demands in the web near (1) the connection stiffener-to-web weld, and (2) the flange-to-web weld, respectively.

A series of influence and envelope surfaces were created to determine load placements for creating maximum web gap stress demand. Based on the envelope and influence surface analysis of the three bridge configurations, it was determined that to produce maximum web gap stresses the fatigue truck loading pattern should be centered over an interior girder in the positive

moment region. Two truck load cases were considered for each bridge examined within the parametric analyses.

The parametric analyses showed that web gap stresses were highly related to cross-frame and connection stiffness. Therefore, during the analyses, great care was taken to “match” the cross-frame and connection stiffness between models so that skew angle and cross-frame spacing could be evaluated independently of cross-frame and connection stiffness. However, a series of skewed-parallel bridge layout models was studied in which cross-frames were sized according to common State DOT practices, utilizing a maximum slenderness limit of L/r = 140.

Focusing on all bridge configurations with cross-frames spaced at 4.57 m (15.0 ft), it was found that skewed-unstaggered configurations exhibited the lowest HSS#1 magnitudes (excluding the skewed-parallel models with (L/r)-based cross-frame stiffness). However, HSS#2 was highest in skewed-unstaggered configurations, highlighting the importance of considering both potential crack locations when evaluating risk of distortion-induced fatigue.

In bridge configurations with 4.57 m (15.0 ft) cross-frame spacing, HSS#1 was higher in skewed-parallel than in skewed-staggered bridge configurations, which suggests that skewed-staggered bridges may be less susceptible to distortion-induced fatigue than skewed-parallel bridges. This is contrary to the common perception that skewed-parallel bridge configurations are less susceptible to distortion-induced fatigue. Because the cross-frame stiffness was maintained nearly constant between models regardless of cross-frame layout, it is important to note that design provisions adopted by most DOTs would lead to cross-frames with different lateral stiffness for the skewed and non-skewed bridge configurations, and that models with skewed-parallel configurations and "L/r-only" cross-frame sizes exhibited lower HSS#1 magnitudes than either the skewed-staggered or skewed-parallel layouts with matched cross frame stiffness. Although this finding supports the practice of using skewed-parallel layouts for bridge configurations with skew angles greater than 20 degrees when the cross-frames are proportioned on the basis of the slenderness ratio (L/r) and commonly-used connection plate dimensions are utilized, caution must be exercised to ensure that the increased flexibility of the cross-frames is sufficient to provide lateral stability to the girders during the construction phase of the bridge and in negative bending regions through the life of the bridge. In these instances it

is also important to verify that the reduced ability to distribute live loads through the cross-frames is properly factored in the design of the girders.

Relative HSS#2 magnitudes were similar for all cross-frame spacings evaluated, with skewed-staggered bridge configurations producing the lowest stresses. HSS#1 also had similar maxima for all cross-frame spacings except 2.29 m (7.50 ft). Skewed-staggered bridge configurations had higher HSS#1 than skewed-parallel bridge configurations for models with cross-frames spaced at 2.29 m (7.50 ft).

Additional details and results are discussed in Appendix D.1. Results from a similar parametric analysis are described in Appendix D.2. An important finding brought forward in this portion of the research was that regions of greatest differential deflection between girders did not reliably correlate with the greatest web gap stress demand. Since prior research has often referred to differential deflections as a driver of distortion-induced fatigue, this caveat was an important finding, and should prompt investigators to consider web gap stresses independently from differential deflections.

Chapter 5: Conclusions and Recommendations

5.1 Angles-with-Plate Retrofit

The angles-with-plate repair was investigated through physical tests performed on girder models (14 test trials) and on the approximately half-depth-scale test bridge (14 test trials). Additionally, high-resolution finite element models were used to perform parametric analyses of the retrofit measure and to compare performance of the angles-with-plate retrofit against various baseline cases (e.g., unretrofitted; retrofitted with the angles-to-top flange technique). Findings from this portion of the study have led to the following conclusions and recommendations:

5.1.1 From the Numerical Analyses:

- Overall, simulations performed for the test bridge and the girder segments showed that the angles-with-plate retrofit can be expected to decrease stress demand at the connection plate-to-web-weld and the flange-to-web weld significantly. The level of stress decrease was found to be dependent upon crack type (connection plate-to-web-weld vs. web-to-flange weld), crack length, and retrofit stiffness.
- A parametric study was performed for the girder models, and it was found that the angles-with-plate retrofit was most effective when stiff angles were used in conjunction with a stiff back plate. For this reason, the test bridge FE models included only stiff versions of the retrofit.
- Finite element models of the test bridge showed that the configuration of the angles-with-plate retrofit that included stiffeners was the most effective variation of the angles-with-plate retrofit measure at reducing stresses in the web gap region. This finding supports the previous conclusions, which also indicated that stiffer retrofits performed better than more flexible retrofits.
- The effects of crack length on retrofit effectiveness are described in the following conclusions, in which results reported for both the test bridge and the girder segments are for stiff versions of the retrofit measure:
    - Models of the test bridge showed that for a crack near the connection plate-to-web weld (unretrofitted): the stress demands at the web-to-flange weld and at the connection plate-to-web weld tended to decrease as crack length increased. Models of the girder models showed that stress demands increased around the connection plate-to-web weld until crack lengths reached approximately 50 mm (2 inches), at which point stresses began to decrease.

- Models of the test bridge showed that for a crack at the web-to-flange weld (unretrofitted): Stress demands at the web-to-flange weld and at the connection plate-to-web weld tended to decrease as crack length increased. Models of the girder subassemblies showed that stress demands increased with increasing crack length. This disparity is likely due to differences between the test set-ups.
- Models of the test bridge showed that for relatively short horseshoe-shaped cracks [25 to 50 mm (1 to 2 inches)], stresses around the connection plate dropped approximately 70% after the retrofit measure was installed and stresses near the flange-to-web weld dropped 35% when a stiff angles-with-plate retrofit was applied. Models of the girder subassemblies showed that the stresses decreased 80% or more near the connection plate-to-web weld after retrofitting short cracks.
- Models of the test bridge showed that for relatively short flange weld cracks [25 to 50 mm (1 to 2 inches)], stresses around the connection plate dropped approximately 65% after retrofitting and stresses around the flange weld dropped approximately 55%. Models of the girder segments showed that stresses around the web-to-flange weld decreased 75-80% after short cracks were retrofitted [for 25 to 50 mm (1 to 2 inches)] crack lengths). For very short crack lengths [13 mm ($^1/_2$ inch)], negligible stress decreases were noted around the web-to-flange weld in the girder segment models.
- Models of the test bridge showed that retrofit effectiveness decreased for both regions of crack susceptibility (at the flange weld, and at the connection plate weld) as the horseshoe-shaped crack length increased, in the presence of only a horseshoe-shaped crack around the connection plate-to-web weld. Models of the girder segments showed an opposite trend for the connection plate-to-web weld, in that the retrofit became more effective with increasing crack length.
- Models of the test bridge showed that retrofit effectiveness decreased for the connection plate weld as crack length increased, in the presence of only a longitudinal crack. The reduction in stress from the cracked & unretrofitted state to the cracked & retrofitted state for the connection plate-to-web weld was approximately 5% for a 203 mm (8 inches) longitudinal crack and 64% for a 25 mm (1 inch) crack. For the flange-to-web weld location, stress reduction due to retrofitting did not vary

significantly with increasing crack length at the flange. Models of the girder segments showed that the angles-with-plate retrofit became slightly less effective at mitigating fatigue stresses around the web-to-flange weld when crack lengths increased.

- From the models of the test bridge and the girder segments, use of stiff angles in conjunction with stiff back plate is recommended for angles-with-plate installation.

5.1.2 From the Physical Tests in the Test Bridge:

- Measurements taken with LVDTs and string potentiometers showed that out-of-plane web gap rotations were significantly decreased after top web gaps were retrofitted using the angles-with-plates technique, indicating a lower distortion-induced fatigue demand on the web gap region.
- When the angles-with-plate retrofit was applied over top web gap regions with existing sharp cracks, horseshoe-shaped crack growth was significantly slowed. Maximum unretrofitted crack growth was observed to be 25 mm (1 inch) over 150,000 cycles at 27-267 kN (6-60 kip) load while maximum retrofitted crack growth was observed to be 11 mm ($^{7}/_{16}$ inch) over 1,200,000 cycles at 36-356 kN (8-80 kip) load.
- When the angles-with-plate retrofit was applied over top web gap regions with horseshoe-shaped cracks that had been modified with small crack-arrest holes drilled at the crack tips, crack growth was halted under 44-445 kN (10-100 kip) loading with a maximum longitudinal bending stress due to fatigue (in the girder's bottom flange) of 48.3 MPa (7.0 ksi).
- In Trials 6N and 7N, unstable crack growth was noted at the web-to-flange weld on the north girder. The crack was not detected until it had reached over 254 mm (10 inches) in length. It is possible that its lack of detection was due to its extremely small crack opening displacement, and it is alternatively possible that the crack formed suddenly between the regular inspections. The influence of the cross-frame fracture that occurred in Trial 4 on the formation of this crack was unclear even after finite analyses were performed of this condition, but it is possible that sudden load redistribution or energy release played a role in the severity of this crack. The crack was not arrested using the angles-with-plate repair in this configuration. This is attributed to the extremely high load levels and the long length of the crack when it was first detected. It is also noted here that no

web-to-flange weld cracking was detected throughout the seven test trials in the south girder.

- During the course of all the test trials, only minimal levels of crack propagation were noted around the connection plate while the angles-with-plate retrofit was present. This coincided with two fatigue failures of the cross-frame tab plates, indicating the excellent performance of the angles-with-plate retrofit under extremely high load levels.

5.1.3 From the Physical Tests of Girder Models:

- Girders in which the angle-with-plates retrofit measure was implemented experienced negligible crack growth under the same load range that caused severe fatigue damage to the web gap region of unretrofitted specimens.
- Experimental results from girder subassemblies under fatigue loading were consistent with the corresponding computer simulations. Areas in the web gap region of computer models exhibiting the highest maximum principal stress demands correlated closely with the locations in which fatigue cracks were observed in the experiments. The manner in which fatigue cracks propagated during experimental simulations of girder subassemblies was also consistent with the results from the computer simulations. Both computer simulations and girder tests showed that there were two primary crack types that formed in the web gap region: a horseshoe-shaped crack along the toe of the weld between the CP and the girder web, and a horizontal crack along the toe of the weld between the web and girder flange.
- Experiments showed that the angles-with-plate retrofit measure was effective in preventing the distortion of the web gap region, drastically reducing the stress demands at critical points. Subassemblies repaired using the angles-with-plate retrofit measure were able to exceed the number of cycles corresponding to infinite fatigue life for AASHTO Category A fatigue details without any measurable crack growth. This result was repeated for girders with various crack lengths, which indicates that, for the ranges evaluated experimentally, the performance of the repair method investigated was not sensitive to the length of the fatigue cracks.
- Although undersized crack-arrest holes were effective for removing the sharp crack tips, experimental results showed that this type of stop-gap measure did not lead to a meaningful increase in fatigue life. This finding is consistent with FE simulations results described in the companion paper, which showed that crack-

arrest holes of this size had a small effect on the calculated stress demand in the web gap region. The observed number of cycles to fatigue-crack re-initiation was comparable to the number of cycles to fatigue crack initiation in the unretrofitted configuration, and an order of magnitude lower than the number of cycles without any measurable crack growth undergone by specimens retrofitted with the angles-with-plate repair.

5.2 Fiber Reinforced Polymer Retrofit Measures

Various repairs utilizing Fiber Reinforced Polymer (FRP) materials were investigated through physical tests performed on small-scale bending specimens, small-scale tension specimens, and girder subassemblies. These tests included the use of carbon fiber reinforced polymer (CFRP) overlays bonded over cracked and uncracked details, FRP blocks cast in web gaps, and a sandwich composite in which CFRP sheets were bonded to a girder web and connection plate and steel angles and backing plate bolted over the CFRP layer. Each of these physical test series was complemented with findings from computational simulations performed using the commercially-available finite element modeling software, Abaqus (SIMULIA 2008). Findings from these investigations have led to the following conclusions:

- Fatigue tests and FE models of CFRP overlays bonded to steel plate loaded in tension showed that using CFRP overlays to repair cracks in steel members can be a highly-effective means of reducing the stress demand and greatly prolonging the fatigue-crack propagation of the steel substrate being tested. Fundamental research performed as part of this study showed that the greatest benefit of using overlays to reduce stress demands was achieved for stiffness ratios below unity. For specimens in which this ratio was maintained, no debonding events were experienced during fatigue testing under extremely high stress ranges.
- Fatigue tests and FE models of plate-cover plate specimens reinforced with CFRP overlay elements showed that the overlays used were able to increase the stiffness of the connection and inhibited crack initiation. Given that achieving increased fatigue life was dependent upon maintaining bond between the steel and CFRP overlay, significant attention was paid to the bond layer. Installation techniques, including the addition of polyester fibers to the resin layer and extending the resin layer beyond the footprint of the overlay, were found to correspond with bond lives between the CFRP and the steel that exceeded the infinite fatigue life threshold of the AASHTO fatigue design curves for the stress range evaluated.

Based on observations of the tests and finite element analyses performed, it is recommended that a fibrous resin captivation layer and an extended interface layer be used during implementation of this repair technique for maintaining adequate bond under cyclic loading. The experimental results also showed that an interface resin layer with a thickness of 6.4 mm ($^1/_4$ in.) and a resin captivation layer comprised of polyester breather cloth provided the best balance of stiffness and bond tenacity for the CFRP overlay elements studied. Results showed that use of CFRP materials to improve the fatigue performance of existing structures is a promising and viable technology. Since achieving satisfactory bond performance has historically been a major hurdle to successfully using CFRP as a fatigue retrofit in steel structures, this was a significant contribution of this study.

- Fatigue testing and FE models of a girder segment loaded in distortion-induced fatigue and retrofitted with a fiber reinforced polymer (FRP) block showed that the retrofit was successful in drastically slowing the rate of crack propagation in the girder. A simple bolted connection was utilized in addition to the bond between the FRP and the steel, to ensure that the retrofit remained engaged with the steel girder throughout testing. This retrofit was developed and tested to determine in an overall sense if FRP repairs could be applied successfully to resist distortion-induced fatigue loading. This research showed that this approach is viable.
- The concept of repairing deep web fatigue cracks with a CFRP-steel sandwich composite was investigated through a physical test sequence and complementing FE analyses. In this study, a modified angles-with-plate retrofit was tested on a physical girder specimen that had sustained very deep fatigue cracks. In the physical tests, two versions of the modified angles-with-plate were tested: one was a steel-only retrofit, and one utilized a layer of CFRP sandwiched between the steel elements and the steel girder; in the latter approach, the CFRP was bonded to the steel with resin, and entire assemblage was also bolted with high-strength structural fasteners. The deep web cracks did not grow under either retrofit application. Interestingly, the complementing FE analyses showed a significant different between the steel-only and the sandwich composite approaches, with the sandwich composite lowering stresses in the fatigue-susceptible region to a greater degree than achieved with the steel-only approach.
- Overall, the portions of this study aimed at investigating the performance of FRP fatigue retrofits showed that FRP materials can be used successfully to repair fatigue cracking due to in-plane tensile loading, in-plane bending loading, and

distortion-induced fatigue loading. In each of these loading scenarios, challenges with bonding strength were addressed and overcome. This study has laid significant groundwork towards field implementation of FRP retrofits as a means to counter the effects of distortion-induced fatigue. The authors of this report recommend that environmental variables be addressed through future research.

5.3 PICK Technology

The PICK device was developed and its effectiveness in extending the fatigue life of drilled crack arrest holes was measured by performing fatigue testing on treated and untreated specimens; measuring retained expansion in treated holes; measuring hardness values around treated and untreated holes; and using neutron diffraction to measure residual stresses around a PICK-treated hole. In addition to considering PICK-treated and untreated specimens, specimens were also included in the test matrix that were treated with pressure-only. The following conclusions resulted from this study:

- A 4% expansion of crack stop holes in steel plates was found to have a very similar effect to that observed in aluminum plates. This conclusion is based on the similarity of normalized tangential residual stress for both materials. This was an important finding, because it helps to provide a meaningful link between existing research performed in the aerospace engineering literature and current needs within the field of bridge engineering. Results from the 2-D and 3-D uniform expansion modeling can be interpreted to be independent from the particular technique chosen to cold-expand undersized crack stop holes, and can be used in future studies to corroborate detailed finite element analyses and experimental findings for specific techniques applicable to steel bridges.
- The performance of untreated control specimens tested in fatigue corresponded to AASHTO fatigue categories of C and B'.
- Treating specimens with pressure-only (simple expansion of the drilled hole) was found to increase the fatigue performance of specimens with drilled holes beyond that of untreated specimens. Pressure-only specimens exhibited performance consistent with AASHTO fatigue categories B' and B.
- Treating specimens with PICK technology further increased the fatigue performance of specimens with drilled holes beyond that of the pressure-only treated specimens. PICK-treated specimens performed at a level consistent with

AASHTO fatigue categories B and A, indicating a performance increase of approximately two categories beyond that of untreated specimens.

- The average *RE* measurements for both treatment techniques examined indicate that *RE* values were well above the 4% threshold shown to be effective in improving the fatigue life of drilled holes.
- The *RE* values measured for PICK-treated drilled holes were higher, on average, than pressure-treated drilled holes.
- The retained expansion values were in good agreement with the fatigue test results. PICK-treated specimens out-performed pressure-only treated specimens in terms of fatigue life and had higher levels of *RE*.
- The metallurgical investigation showed increasing levels of grain deformations between the pressure-only and PICK-treated specimens, which supports the conclusions from the fatigue tests and the *RE* measurements.
- Neutron diffraction measurements showed levels of compressive tangential residual strains consistent with those computed using closed-form solutions, and are great enough in magnitude to produce a fatigue-protection effect.

This portion of TPF-5(189) has shown the merit of pressure-treating drilled holes in bridges to increase the fatigue performance, providing the fundamental groundwork for additional research to be performed on larger scale specimens. Additionally, this research has shown that ultrasonic treatment using PICK technology can be used to further improve the fatigue performance of drilled holes in bridges through a combination of cold expansion and cold-working. Solutions such as these can be used for existing steel bridges susceptible to fatigue cracking (drilled crack-arrest holes) to extend the useful life of the nation's infrastructure.

5.4 Cross-Frame Layout and Skew Effects

The effects of skew angle, cross-frame spacing, bracing layout, cross-frame stiffness, and load placement on bridge susceptibility to distortion-induced fatigue were evaluated by performing more than 1,000 analysis jobs of high-resolution 3D finite element models. The following conclusions were reached by analyzing the results of the computer simulations:

- Differential deflection and stress were found to be proportional, although differential deflection did not predict the row of cross frames corresponding with the highest web gap stress demand.

- Maximum differential deflections and stresses occurred in positive moment regions for all of the bridges modeled.
- Maximum stresses consistently occurred in the top web gap region of the exterior girder adjacent to the loaded girder (Girder 4) in bridges with cross frames placed parallel to skew angle.
- Maximum stresses consistently occurred in the bottom web gap region of the loaded girder (Girder 3) in bridges with staggered cross frames. Therefore, it was found that bottom web gaps should not be neglected in analysis, and should be considered during fatigue life assessment of existing structures.
- Two distinct locations prone to the initiation of fatigue cracks were identified in the web gap region; one at the connection stiffener-to-web weld (HSS#1) and another at the flange-to-web weld (HSS#2). Both are important in assessing the vulnerability to fatigue damage and should be examined independently.
- Maximum HSS magnitudes occurred in top web gaps of girders in regions of positive bending when cross-frames were placed back-to-back, but occurred in bottom web gaps of skewed-staggered bridge configurations. Maximum HSS was always produced when loads were placed on the bridge deck above the intersection of a cross-frame and girder web.
- Bridges with cross frames placed parallel to the skew angle and those with staggered cross frames behaved very differently, although the maximum stress was found to be similar for both brace placements considered.
- In bridges with cross frames placed parallel to the skew angle, increased cross frame spacing slightly increased the maximum stress in the bridge.
- Stagger and cross frame spacing had a large impact on the stresses in the web gap region of bridges with staggered cross frames, although the stress values did not increase proportionally to skew angle.
- In bridges with staggered cross frames, the restraint placed on the girder by the cross-frames was found to be a significant parameter in the location and magnitude of web gap stresses.
- In skewed-parallel bridge configurations, the stress demand at the web-to-stiffener weld (HSS#1) increased with skew angle, while the stress demand at the web-to-flange weld (HSS#2) decreased with skew angle. Skew angle did not have a significant effect on HSS in skewed-unstaggered bridge configurations.
- Increases in cross-frame spacing in non-skewed, skewed-parallel, and skewed-unstaggered bridge configurations led to increased HSS at both weld locations (HSS#1 and HSS#2). For the bridge configurations analyzed in this study it was

found that this effect became negligible when the cross-frame spacing exceeded 6.86 m (22.5 ft) as evidenced by the fact that HSS magnitudes were similar for bridges with cross-frames spaced at 6.86 m (22.5 ft) and 9.14 m (30.0 ft).

- Out-of-plane girder deflections had a very significant effect on the location and magnitude of the HSS in skewed-staggered bridge configurations. The out-of-plane girder deflections were proportional to the flexibility of the girder with respect to bending about the weak axis and torsion, which were related to cross-frame spacing or the skew angle.
- Stiffness of both cross-frame elements and connection stiffeners had a significant impact on the susceptibility to distortion-induced fatigue and was found to be as important as other evaluated parameters, including skew angle and cross-frame spacing. Larger cross-frame and connection plate sizes corresponded with increased web gap HSS.
- In skewed-parallel bridges with “L/r only” cross-frames spaced at 4.57 m (15.0 ft), HSS did not increase with skew angle. Instead, bracing became more flexible with the increased skew angle, and was less effective in load transfer. Subsequently, distortion-induced fatigue susceptibility was lessened; however, the reader is cautioned that skewed bracing should also be designed considering lateral stability demands of the girders.
- Given the relationship that was found between cross-frame stiffness and web gap HSS, the relative stiffness of the cross-frames within a bridge may control the region of the bridge most susceptible to distortion-induced fatigue cracking. This may be one reason previous literature presents conflicting conclusions regarding the region of the bridge most vulnerable to distortion-induced fatigue.

It should be noted that other parameters such as geometric properties of the bridge and the characteristics of the slab also may have a significant effect on distortion-induced fatigue damage and that the findings of this study are not intended to imply otherwise. Future research should carefully examine other bridge parameters to determine their effects upon distortion-induced susceptibility. Additionally, research is needed in the area of curved and skewed-curved bridges to determine susceptibility of such systems to distortion-induced fatigue, although the number of affected bridges is likely to be small. Finally, the authors would like to stress the importance of field observation to follow the analytical study described in this paper.

5.5 Summary

TPF-5(189) has resulted in a collection of newly-developed retrofit techniques to control distortion-induced fatigue cracking in steel bridges. The common thread between these retrofits is that they are intended to be installed while the bridge is operating normally. Furthermore, the set of repair techniques developed evaluated the use of new materials and technologies to repair fatigue damage. The techniques developed and tested under TPF-5(189) include: angles-with-plate repair technique, FRP composite block, steel-FRP sandwich repair, and PICK technology. These techniques have performed extremely well under demanding fatigue testing at high load levels.

Of the techniques developed, the angles-with-plate technique is the most field-ready, and should result in significant cost savings to the bridge owner where its application is appropriate. Extensive analytical and experimental testing has shown that the angles-with-plate retrofit technique is highly effective in arresting cracking occurring around the connection plate-to-web weld. Performance of the angles-with-plate retrofit at mitigating crack growth was shown to be best when the angles were very stiff in relation to the girder web. A version of the angles-with-plate retrofit that included stiffeners exhibited excellent performance in analyses and physical tests. It is recommended that carefully-monitored field applications of this technique be performed to further verify its performance in mitigating distortion-induced fatigue. It is noted here that the authors are engaged with the KDOT in a separate study in which the performance of the angles-with-plate retrofit is being studied in a highway bridge field application.

This study has brought the use of FRP materials as a repair technique for fatigue in steel bridges significantly closer to field-readiness. The technologies tested performed extremely well in analytical and demanding physical fatigue tests. Problems with bond durability that have been the primary historical obstacle to FRPs being used as a fatigue retrofit were overcome. Both the bond layers and the CFRP applications were significantly different from techniques that have been used by other researchers, and show great promise for field application. The research gap that remains pertaining to use of the FRP technologies is environmental durability. The authors recommend that future work be performed, either in the lab or in a closely-monitored field application, in which the FRP techniques are exposed to normal environmental demands. It is

worth noting that the two FRP retrofits developed for distortion-induced fatigue include not only a resin bond layer, but also a bolted connection; this mechanism should help to alleviate concerns of a retrofit failure due to environmental factors while still maintaining the benefits of a resin layer between the CFRP and steel.

PICK technology was developed under TPF-5(189) for treating the inside surface of drilled crack-arrest holes. Of the multiple technologies developed under this study, this was the 'highest-risk' concept pursued. This portion of the study resulted in a bench-scale device that was shown through fatigue testing, metallurgical evaluation, neutron diffraction measurements, and extensive finite element modeling to be an effective technique. It is recommended that further research and development be pursued to modify the device to a field-ready technology.

TPF-5(189) has also resulted in a deeper understanding of the factors driving distortion-induced fatigue in both straight and skewed bridges, as well as which types of commonly-used repairs may be most useful depending on cross-frame layout and skew angle.

In summary, TPF-5(189) has resulted in the development of a broad range of new technologies for repairing distortion-induced fatigue in steel bridges that are expected to bring about significant cost-savings for bridge owners and reduce bridge closures during repairs as they can be performed while the bridge remains open to traffic.

References

American Iron and Steel Institute (AISI) Example 2: Two-Span Continuous Composite I Girder (1997). American Iron and Steel Institute, Washington, D.C.

American Association of State Highway and Transportation Officials (AASHTO). (2013). *2013 Interim Revisions to the AASHTO LRFD Bridge Design Specifications.* 6th ed. AASHTO, Washington, D.C.

ASTM E140-12 (2012). Standard Hardness Conversion Tables for Metals Relationship Among Brinell Hardness, Vickers Hardness, Rockwell Hardness, Superficial Hardness, Knoop Hardness, Scleroscope Hardness, and Leeb Hardness. ASTM International, West Conshohocken, PA.

Ball, D.L. (1995). *Elastic-Plastic Stress Analysis of Cold Expanded Fastener Holes*. Fatigue and Fracture of Engineering Materials and Structures, Vol. 18, Issue 1.

Barth, A. S. and Bowman, M. D. (2001). "Fatigue Behavior of Welded Diaphragm-to-Beam Connections." *Journal of Structural Engineering*, 127(10), 1145-1152.

Berglund, E. and Schultz, A. (2006). "Girder Differential Deflection and Distortion-Induced Fatigue in Skewed Steel Bridges." *Journal of Bridge Engineering*, 11(2), 169-177.

Connor, R. J. and Fisher, J. W. (2006). "Identifying Effective and Ineffective Retrofits for Distortion Fatigue Cracking in Steel Bridges Using Field Instrumentation." *Journal of Bridge Engineering*, 11(6), 745-752.

Dexter, R. and Ocel, J. (2013). *Manual for Repair and Retrofit of Fatigue Cracks in Steel Bridges*. Publication no. FHWA-IF-13-020. Federal Highway Administration, McLean, VA.

Fisher, J. W., Jian, J., Wagner, D. C., and Yen, B. T. (1990). *Distortion-Induced Fatigue Cracking in Steel Bridges*. NCHRP Report 336. Transportation Research Board, National Research Council, Washington, D.C.

Fisher, J. W. and Keating, P. B. (1989). "Distortion-Induced Fatigue Cracking of Bridge Details with Web Gaps." *Journal of Constructional Steel Research*, 12(3-4), 215-228.

Fraser, R. E. K., Grondin, G. Y., and Kulak, G. L. (2000). *Behaviour of Distortion-Induced Fatigue Cracks in Bridge Girders*. Structural Engineering Report no. 235. University of Alberta, Edmonton, Canada.

Jones, J., Bennett, C., Matamoros, A., Rolfe, S., and Roddis, K. (2008). "Fighting Fatigue in Steel Bridges." *TR News* 259, 25-26. Transportation Research Board, Washington, D.C.

Kaan, B., Barrett, R., Bennett, C., Matamoros, A., and Rolfe, S. (2008). "Fatigue Enhancement of Welded Coverplates Using Carbon-Fiber Composites." *2008 ASCE/SEI Structures Congress Proceedings*, 1-8.

Khalil, A., Wipf, T. J., Greimann, L., Wood, D. L., and Brakke, B. (1998). “Retrofit Solution for Out-of-Plane Distortion of X-Type Diaphragm Bridges.” *Transportation Conference Proceedings, Iowa Department of Transportation*, 99-102.

Li, H. and Schultz, A. E. (2005). *Analysis of Girder Differential Deflection and Web Gap Stress for Rapid Assessment of Distortional Fatigue in Multi-Girder Steel Bridges: Final Report*. MN/RC-2005-38. Minnesota Department of Transportation, St. Paul, MN.

Moniz, B. J. (1994). *Metallurgy*. 2nd ed. American Technical Publishers, Inc., Homewood, IL.

Nadai, A. (1943). *Theory of Expanding of Boiler and Condenser Tube Joints through Rolling*. Transaction of the American Society of Mechanical Engineers, Vol.65, Issue 8.

Quadrato, C., Battistini, A., Helwig, T., Engelhardt, M., and Frank, K. (n.d.) “Effect of Cross Frame Connection Details on Stability of Steel Bridges with Skewed Supports.” http://www.aisc.org/assets/0/1209478/1209480/1271820/39248d5d-83ad-4575-ae4c-4672c2486359.pdf. Accessed 12/16/2009.

SIMULIA (2008). Abaqus, Version 6.8-2. http://www.simulia.com.

Stallings, J. M., Cousins, T. E., and Stafford, T. E. (1999). “Removal of Diaphragms from Three-span Steel Girder Bridge.” *Journal of Bridge Engineering*, 4(1), 63-70.

Tedesco, J. W., Stallings, J. M., and Tow, D. R. (1995). “Finite Element Method Analysis of Bridge Girder-Diaphragm Interaction.” *Computers and Structures*, 56(2-3), 461-473.

AD ASTRA PER ASPERA

Kansas

Department of Transportation